Spectral Analysis of Electromagnetic Diffraction Phenomena in Angular Regions Filled by Arbitrary Linear Media

MDPI

Article

Spectral Analysis of Electromagnetic Diffraction Phenomena in Angular Regions Filled by Arbitrary Linear Media

Vito G. Daniele [1,†], Guido Lombardi [2,*,†] 0000-0002-7311-2279

[1] DET, Politecnico di Torino, Torino, Italy; vito.daniele@polito.it
[2] DET, Politecnico di Torino, Torino, Italy; guido.lombardi@polito.it
* Correspondence: guido.lombardi@polito.it; Tel.: +39-011-0904012
† These authors contributed equally to this work.

Abstract: A general theory for solving electromagnetic diffraction problems by impenetrable/penetrable wedges immersed in/made of an arbitrary linear (bianistropic) medium is presented. This novel and general spectral theory handles complex scattering problems by using transverse equations for layered planar and angular structures, characteristic Green's function procedure, Wiener-Hopf technique, and a new methodology to solve GWHEs. The technique has been proved effective for the analysis of wedge problems immersed in isotropic media and, in this paper, we extend the theory to more general cases providing all necessary mathematical tools with validation. We obtain Generalized Wiener-Hopf equations (GWHEs) from spectral functional equations in angular regions filled by arbitrary linear media. The equations can be interpreted with network formalism for a systematic view. We recall that spectral methods (such as the Sommerfeld-Malyuzhinets (SM) method, the Kontorovich-Lebedev (KL) transform method, and the Wiener-Hopf (WH) method) are well consolidated fundamental and effective tools for the correct and precise analysis of electromagnetic diffraction problems constituted of abrupt discontinuities immersed in media with one propagation constant, although not immediately applicable to multiple propagation constant problems. According to our opinion, for the first time, the proposed mathematical technique extends the possibilities of spectral analysis of electromagnetic problems in presence of angular regions filled by complex arbitrary linear media providing novel mathematical tools. Validation through fundamental examples is proposed.

Keywords: wave motion, diffraction, electromagnetism, arbitrary linear media, bianisotropic media, layered media, applied mathematics, Green's function, Wiener-Hopf method, integral equations, Fredholm factorization.

Citation: Daniele, V.G.; Lombardi, G. Spectral Analysis of Diffraction Phenomena in Angular Regions Filled by Arbitrary Linear Media. *Journal Not Specified* **2023**, *1*, 0. https://doi.org/

Received:
Revised:
Accepted:
Published:

1. Introduction

The theory of wave diffraction constitutes one of the fundamental problems in Mathematical Physics. Apart from its direct relevance to Engineering and Physics, this subject gives rise to significant methodologies in Applied Mathematics.

Spectral methods play a crucial role in the study of electromagnetic diffraction. Notably, the Sommerfeld-Malyuzhinets (SM) method, the Kontorovich-Lebedev (KL) transform method, and the Wiener-Hopf (WH) method are fundamental and complementary in studying diffraction problems in presence of sharp discontinuities. These methods have been extensively and effectively applied for studying wedge diffraction in isotropic regions, see references [1–6] for SM, [7–10] for KL, [11–16] for WH and references therein. Moreover, using synergy among the three methods (WH, SM, KL) the authors obtained a complete network representation of angular region in presence of isotropic media [17], that helps to build a systematic methodology of analysis.

The main advantage of the aforementioned techniques (SM,KL) is also one limitation, i.e. the utilization of the spectral complex angular plane derived from the Sommerfeld integral theory [18], which has been effectively used also in WH framework for Fredholm

factorization [12–16,19] and with the definition of rotating waves in isotropic angular region [20],[15,16]. The definition of this complex plane is intricately connected to the physics of the problem, as it specifically requires spectral transformations associated with the propagation constant. Consequently, this methodology is applicable to problems involving one single propagation constant, such as isotropic media in electromagnetic fields, as well as other specific problem configurations with decoupling properties in propagation modalities. Different attempts were developed to extend the spectral analysis to diffraction problems in more complex media as for example gyrotropic media and/or uniaxial media. For example, we recall the analysis of scattering by perfect electrically conducting (PEC) half-plane immersed in such anisotropic media, see [21–30]. However, to the best of our knowledge, no spectral method has been developed for scattering problems by wedges in arbitrary linear media (i.e. bianisotropic media [31–33]), characterized by multiple propagation constants. One of the most important result obtained in presence of anisotropic media is the exact solution obtained by Felsen in the case of the scattering by a PEC wedge immersed in uniaxial medium illuminated by plane waves at normal incidence [23,24]. However the method used for this problem is substantially that of the separation of variables after transformations in physical domain and it does not present the powerful characteristics of the spectral methods, such asymptotic evaluation of fields and physical interpretation of field components in terms of structural and source spectral singularities. Other important works examine the behavior of the field near the edge of a wedge immersed in complex media [34] and the diffraction by wedge immersed in the special case of an isotropic chiral medium with SM method [35].

Given our experience in the spectral analysis of complex electromagnetic scattering problems in isotropic media [15,16,36–38], and with the help of the theory proposed in [39,40] for the analysis of structures embedded in layered media, in this work we develop a new theory in spectral domain with proper mathematical tools that allows to represent scattering problems immersed in arbitrary linear media of angular shape. In particular these new formulations are in spectral domain (Laplace domain) without introducing angular complex planes thus not limited to *one-propagation-constant* problems. In [41], we have developed the general theory in abstract form to model angular regions filled by arbitrary linear media and we have reported its implementation for isotropic media.

With the present work, we propose a complete theoretical package for solving diffraction problems by impenetrable wedges immersed in an arbitrary linear medium, extendable to multiple penetrable angular regions. The proposed method exploits the combination and the extension of powerful mathematical tools developed in different contexts. The first tool is the Bresler-Marcuvitz (BM) Transverse Equation Theory for layered media [40,42], the second is the characteristic Green's function procedure [43,44], the third one is the Wiener-Hopf Technique [40,45] in its generalized form [15,16] and the fourth one (which is a completely novel contribution) is the direct application of Fredholm factorization to Generalized Wiener-Hopf equations (GWHEs).

The method starts with an extension of transverse equation theory for layered arbitrary linear media to stratification of angular shape with the help of BM abstract notation. We then apply characteristic Green's function procedure to get solution of equation in angular shaped geometries. The solutions defined at the faces of the angular region are spectral functional equations that relates continuous (tangential) field components of the two faces delimiting an homogeneous angular region. The application of boundary conditions yields system of Generalized Wiener-Hopf equations (GWHEs) where *generalized* means that the definition of the field components of each face are defined into different complex planes but related together. The GWHEs preserve the characteristic form of Classical Wiener-Hopf equations (CWHEs) where the system of equations presents a kernel, plus and minus unknowns; but the plus and minus unknowns are defined into different complex planes (related together). The functional equations and GWHEs of angular regions can be suitably interpreted with network formalism as commonly done in classical layered regions using transmission line theory. This circuit/network modeling representation of angular regions

allows to describe the technique with systematic steps avoiding redundancy. This capability is particular useful when dealing with complex scattering problems where we break down the complexity of the geometry into subdomains of canonical shape. These subdomains are modelled via spectral functional equations or related integral representations that can be interpreted through network approach (obtained once and for all) and are capable to model the entire complex problem by composition of circuital relationships, see for instance [36–38].

In presence of isotropic medium (and further special cases of more general media), a suitable mapping reduces the GWHEs to CWHEs amenable in some cases of exact solutions, alternatively we can resort to the semi-analytical/approximate general-purpose factorization method: the Fredholm Factorization. This technique has been presented in [19] for CWHEs and it has been effectively applied in complex scattering isotropic problems [15,16,36–38].

The main constraint in the present work resides in the complexity of the media that does not allow mappings between complex planes of GWHEs for their transformation into CWHEs. Consequently, in particular when dealing with arbitrary linear media, we propose to rely on a novel version of the versatile approximate method known as Fredholm factorization. Here we apply for the first time the Fredholm factorization method directly to GWHEs as a regularization tool. This regularized method can be derived also before the imposition of boundary conditions, i.e directly on spectral functional equations thus before obtaining the GWHEs of the problem, by reversing the classical order of imposing boundary conditions and then apply Fredholm regularization obtain same effectiveness in the method. We call this new methodology *Direct Fredholm Factorization*.

We observe that the impossibility to map GWHEs to CWHEs in arbitrary linear media is similar to the impossibility to define an unique angular complex plane for SM, KL, and also WH methods, but the new WH methodology proposed in this paper overcomes this obstacle resorting to direct Fredholm factorization applied to GWHEs.

From the solution of the GWHEs inherent to the angular region problem we obtain the spectral representation of field components along the faces delimiting homogeneous angular regions. The complete spectral analysis of the diffraction problems is then obtained resorting again to spectral functional equation written for an arbitrary azimuthal direction. Finally, spectral inversion yields field components in physical domain for any point in the angular regions. An alternative method to get the field is also proposed and it is based on the use of superposition (because of linearity) on spectral representations before spectral inversion, identifying spectral contributions of the faces of the angular regions using equivalence theorem.

All the theoretical properties of the mathematical statements are fully described in the text, although sometimes complete rigorous mathematical proofs are limited. On the other hand, validation-through-examples of the proposed novel theoretical package is reported, starting from demonstrating effectiveness of direct Fredholm factorization applied to GWHEs in the scattering from a PEC wedge immersed in an isotropic medium and, ending with validation of functional equations of angular regions in arbitrary linear media with the analysis of a PEC half-plane immersed in particular anisotropic media.

While implementing the method, we observe that the main difficulty resides in the correct estimation of kernel functions in the GWHEs and the corresponding FIE formulations for the presence of multivalued functions that need particular attention in their definition and calculation. The following Sections highlight all multivalued functions and their correct estimation and assumption.

In summary, we highlight in brief the main novelties of this work with respect to the state of the art reported in the Introduction:

- the development of a first spectral method capable to handle scattering in arbitrary linear media with multiple propagation constants,
- the introduction of a novel solution procedure of GWHEs in particular with multiple propagation constants: the Direct Fredholm Factorization,

- the description in terms of the network interpretation of spectral functional equations and related integral representations for angular regions filled by arbitrary linear media,
- the computation of the field at each point within the angular region resorting to the equivalence theorem and using Kirchhoff representations in the spectral domain,
- the improvement of quality of approximate spectral solutions re-imposing GWHEs (named iteration).

It is important to highlight that the applicability of the proposed WH technique to arbitrary linear media resides on its formulation directly in the Laplace domain avoiding other complex planes, while techniques, such as SM, use complex angular plane based on Sommerfeld representations that are applicable only to isotropic media or special cases of anisotropic media. Moreover, although also SM uses Fredholm integral equations in complex angular plane for approximate solutions [2,6] but limited to isotropic media, again the proposed WH method is extended to arbitrary linear media with Direct Fredholm Factorization because directly formulated in Laplace domain. Furthermore, another important result is that, while Sommerfeld-Malyuzhinets solutions combined to asymptotic methods require analytical extension of the spectral solutions in the improper sheet to compute far field, the proposed application of equivalence theorem in the context of the proposed method can be directly applied to approximate WH spectral solutions in Laplace domain. This result is due to the fact that the direct solution of the GWHE equations provide also the complete spectra of the field on the two faces of an angular region useful for asymptotic estimations.

This article is organized into seven Sections and one Appendix. In Section 1, we introduce the motivation and the scope of the present work and report on the state of the art related to the spectral analysis of diffraction in complex media. Section 2 presents the main mathematical steps to get spectral functional equations in angular region filled by an arbitrary linear media and with arbitrary boundary conditions starting from BM abstract notation for transverse equation in layered planar regions and by extending this theory to layered angular regions filled by arbitrary linear media. Section 3 develops the theory starting from spectral functional equation to get regularize integral representations for angular regions in arbitrary linear media with direct application of Fredholm factorization method. If boundary conditions are applied the representations are GWHEs. Section 4 presents the route to get asymptotic estimation of far field inside the angular region once the face spectra on the two limiting faces is obtained. To demonstrate the efficacy of the proposed methodology, in particular the direct Fredholm factorization, Section 5 reports validation in the simple case of a PEC wedge immersed in an isotropic medium. To further validate the method in arbitrary linear media, Section 6 presents an example of application of functional equations in arbitrary linear media: PEC half-plane immersed in a gyrotropic medium, then we have conclusions. Section 7 contains conclusions and the Appendix reports the full explicit formulas and equations when abstract notation is used in the main text with the dual purpose of enhancing readability and ensuring completeness.

2. Spectral Functional Equations in Angular Region Filled by Arbitrary Linear Media

Spectral functional equations in angular regions filled by arbitrary linear media are obtained by exploiting the combination and the extension of powerful mathematical tools developed in different contexts: the Bresler-Marcuvitz (BM) Transverse Equation Theory for layered media [40,42] and the characteristic Green's function procedure [43,44]. In this section, following [41], we first briefly revisit the BM theory for layered planar arbitrary linear media as a fundamental step to analyze layered angular regions. We then apply the characteristic Green's function procedure to get solutions of the obtained system of differential equations. Finally, we provide the spectral functional equations by evaluating the solution at the faces of the angular region. In particular the functional equations relates continuous (tangential) spectral field components defined at the two faces of the angular region.

We start from the application of BM theory to Maxwell's equations in layered arbitrary non-dispersive homogeneous linear media with tensorial constitutive relations (i.e. bianisotropic media [31–33])

$$\begin{aligned} \boldsymbol{D} &= \underline{\underline{\boldsymbol{\varepsilon}}} \cdot \boldsymbol{E} + \underline{\underline{\boldsymbol{\xi}}} \cdot \boldsymbol{H} \\ \boldsymbol{B} &= \underline{\underline{\boldsymbol{\zeta}}} \cdot \boldsymbol{E} + \underline{\underline{\boldsymbol{\mu}}} \cdot \boldsymbol{H} \end{aligned} \tag{1}$$

where the electric and magnetic fields $(\boldsymbol{E}, \boldsymbol{H})$ are related to the electric and magnetic fluxes $(\boldsymbol{D}, \boldsymbol{B})$ and, the tensors $(\underline{\underline{\boldsymbol{\varepsilon}}}, \underline{\underline{\boldsymbol{\mu}}}, \underline{\underline{\boldsymbol{\xi}}}, \underline{\underline{\boldsymbol{\zeta}}})$ are respectively the electric permittivity, the magnetic permeability, the two magneto-electric coupling parameters.
By assuming

a) Cartesian coordinates (z, x, y)
b) $e^{+j\omega t}$ time harmonic field dependence
c) invariant geometry along z and stratification along y
d) sources constituted of plane waves having $z-$dependence $e^{-j\alpha_o z}$ where α_o depends on skewness angle with respect to z ($\alpha_o = 0$ at normal incidence on z)

we obtain the transverse differential equations in matrix form for layered planar media

$$-\frac{\partial}{\partial y}\boldsymbol{\psi_y}(x,y) = \boldsymbol{M_y}(-j\alpha_o, \frac{\partial}{\partial x}) \cdot \boldsymbol{\psi_y}(x,y) \tag{2}$$

where the four dimension column vector[1]

$$\boldsymbol{\psi_y} = |\boldsymbol{E_t^t}, \boldsymbol{H_t^t}|^t, \ \ with\ \boldsymbol{E_t} = |E_z, E_x|^t, \ \boldsymbol{H_t} = |H_z, H_x|^t \tag{3}$$

Based on the nature of Maxwell's equations, $\boldsymbol{M_y}(-j\alpha_o, \frac{\partial}{\partial x})$ is a second order four dimension matrix differential operator of the form:

$$\boldsymbol{M_y}(-j\alpha_o, \frac{\partial}{\partial x}) = \boldsymbol{M}_{yo} + \boldsymbol{M}_{y1}\frac{\partial}{\partial x} + \boldsymbol{M}_{y2}\frac{\partial^2}{\partial x^2} \tag{4}$$

where the explicit forms of the matrices $\boldsymbol{M}_{yo}, \boldsymbol{M}_{y1}, \boldsymbol{M}_{y2}$ for an arbitrarily linear media (1) are reported in the Appendix A at (A2)-(A9). The application of Fourier transform along x reduces (2) to

$$-\frac{d}{dy}\boldsymbol{\psi_y}(\eta,y) = \boldsymbol{M_y}(-j\alpha_o, -j\eta) \cdot \boldsymbol{\psi_y}(\eta,y) \tag{5}$$

where $\boldsymbol{\psi_y}(x,y) \doteq \frac{1}{2\pi}\int_{-\infty}^{\infty} \boldsymbol{\psi_y}(\eta,y)e^{-j\eta x}d\eta$ and

$$\boldsymbol{M_y}(-j\alpha_o, -j\eta) = \boldsymbol{M}_{yo} - j\eta\boldsymbol{M}_{y1} - \eta^2\boldsymbol{M}_{y2} \tag{6}$$

We introduce here the analysis of the operator $\boldsymbol{M_y}(-j\alpha_o, -j\eta)$ of the layered planar arbitrarily linear media necessary to get the solution of (2) in terms of eigenvalues, eigenvectors with the characteristic Green's function procedure and boundary conditions. The same study is needed to obtain solution for layered angular arbitrarily linear media. Supposing for the general case (removing exceptions) that $\boldsymbol{M_y}$ is semi-simple, we compute its eigenvalues λ_i and eigenvectors $\boldsymbol{u_i}$

$$\boldsymbol{M_y u_i} = \lambda_i \boldsymbol{u_i} \tag{7}$$

i.e.

$$\boldsymbol{M_y} = \boldsymbol{U_y J_y U_y^{-1}} \tag{8}$$

[1] Throughout the paper we assume notation | | for vectors not for modulus of a vector

where $\boldsymbol{J_y} = diag\{\lambda_1, \lambda_2, \lambda_3, \lambda_4\}$ and $\boldsymbol{U_y} = (\boldsymbol{u_1}, \boldsymbol{u_2}, \boldsymbol{u_3}, \boldsymbol{u_4})$ (dependence on η and α_o is omitted). The computation of eigenvalues is obtained from the zeros of characteristic equation of order four (9) whose coefficients can be written using Bocher's formula [46]:

$$det[\boldsymbol{M_y} - \lambda_i \boldsymbol{I}] = \lambda_i^4 + a\lambda_i^3 + b\lambda_i^2 + c\lambda_i + d = 0 \tag{9}$$

$$a = -tr(\boldsymbol{M_y}),\ b = -\frac{a\, tr(\boldsymbol{M_y}) + tr(\boldsymbol{M_y^2})}{2},\ c = -\frac{b\, tr(\boldsymbol{M_y}) + a\, tr(\boldsymbol{M_y^2}) + tr(\boldsymbol{M_y^3})}{3},\ d = det[\boldsymbol{M_y}] \tag{10}$$

It yields the four eigenvalues:

$$\lambda_1 = -\frac{a}{4} + \frac{\sqrt{T} + \sqrt{M_a + Q}}{2},\ \lambda_2 = -\frac{a}{4} + \frac{\sqrt{T} - \sqrt{M_a + Q}}{2}, \tag{11}$$

$$\lambda_3 = -\frac{a}{4} - \frac{\sqrt{T} + \sqrt{M_a - Q}}{2},\ \lambda_4 = -\frac{a}{4} - \frac{\sqrt{T} - \sqrt{M_a - Q}}{2} \tag{12}$$

where

$$T = \frac{a^2}{4} + \frac{-3ac + b^2 + 12d}{3\sqrt[3]{u}} + \frac{\sqrt[3]{u} - 2b}{3},\ Q = -\frac{a^3 - 4ab + 8c}{4\sqrt{T}},\ M_a = \frac{3a^2}{4} - 2b - T \tag{13}$$

with

$$u = \frac{\sqrt{s} + v}{2},\ v = 9\Big(3a^2d - abc - 8bd + 3c^2\Big) + 2b^3,\ s = v^2 - 4\Big(-3ac + b^2 + 12d\Big)^3. \tag{14}$$

We note that the column vectors $\boldsymbol{u}_{i=1,2,3,4}$ of $\boldsymbol{U_y}$ provide a basis in the space $\mathbb{C}^4$ where we define the transverse electromagnetic field $\boldsymbol{\psi_y}$, while the column vectors $\boldsymbol{v}_{i=1,2,3,4}$ of

$$\boldsymbol{V_y} = \boldsymbol{U_y^{-1}} \tag{15}$$

in the reciprocal space will be fundamental to obtain functional equations through the characteristic Green's function procedure. Each couple $(\boldsymbol{u_i}, \boldsymbol{v_i})$ is related to a single λ_i whose explicit forms are in general the cumbersome expressions reported in (11),(12) and depend on η. In the most simple case, i.e. the isotropic medium ($\underline{\underline{\varepsilon}} = \varepsilon \underline{\underline{\boldsymbol{I}}}, \underline{\underline{\mu}} = \mu \underline{\underline{\boldsymbol{I}}}, \underline{\underline{\xi}} = \underline{\underline{\zeta}} = \underline{\underline{\boldsymbol{0}}}$), λ_i assume the forms

$$\lambda_1 = \lambda_2 = -\lambda_3 = -\lambda_4 = \sqrt{(\alpha_o^2 + \eta^2) - k^2} = j\sqrt{(k^2 - \alpha_o^2) - \eta^2} = j\xi_{iso},\ k = \omega\sqrt{\varepsilon\mu} \tag{16}$$

where in presence of losses ($k = k_r - jk_i$; $k_r, k_i > 0$) we have $\mathrm{Re}[\lambda_{1,2}] > 0$ and $\mathrm{Re}[\lambda_{3,4}] < 0$, i.e. respectively related to progressive ($i = 1, 2$) and regressive ($i = 3, 4$) waves with respect to y of the form $e^{-j\eta x} e^{-\lambda_i y} e^{-j\alpha_o z}$. In this framework we associate the direction of propagation to attenuation phenomena, while we let free of constraint the phase variation to model also left-handed materials. In a general arbitrary (even small) lossy linear medium we have always two eigenvalues, say $i = 1, 2$, with positive real part $\lambda_i = +j\xi_i$ representing progressive waves and two, say $i = 3, 4$, with negative real part $\lambda_i = -j\xi_i$ representing regressive waves, yielding all four y longitudinal propagation constants with $\mathrm{Im}[\xi_i] < 0$[2] (progressive/regressive $e^{\mp j\xi_i y}$).

We affirm here the importance of keeping the generality of the medium, since, while investigating scattering of objects immersed in arbitrary linear media, the scatterer can be arbitrary oriented with respect to the principal axis of the (crystal) medium. However, when the problem allows the definition of a coordinate system which coincides with the principal axes of the crystal medium, we get tensorial constitutive relations with diagonal tensors (1). These media are called biaxial, uniaxial, isotropic while the three terms in

[2] Assuming time-harmonic dependence $e^{+j\omega t}$ we have a x,y,z progressive waves $e^{-j\eta x} e^{-j\xi_i y} e^{-j\alpha_o z}$ respectively with $\mathrm{Im}[\eta, \xi_i, \alpha_o] < 0$

the diagonal are respectively all different, one different, all equal. Other special cases are gyrotropic media that represents medium where the tensorial constitutive relations with respect to the coordinate system are hermitian of the following type (in (17) we limit description to the permittivity, i.e. gyroelectric medium)

$$\underline{\underline{\boldsymbol{\varepsilon}}} = \begin{bmatrix} \varepsilon & +j\varepsilon_g & 0 \\ -j\varepsilon_g & \varepsilon & 0 \\ 0 & 0 & \varepsilon_a \end{bmatrix} \tag{17}$$

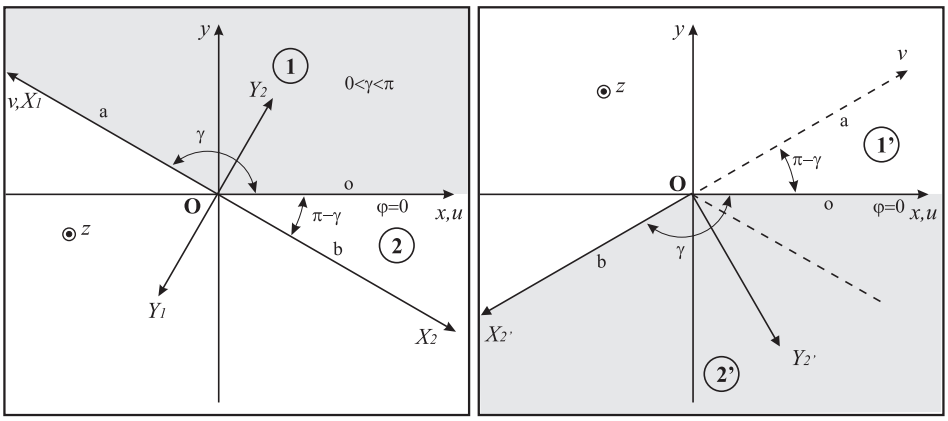

Figure 1. Angular regions and oblique Cartesian coordinates. (a) The figure reports the z, x, y Cartesian coordinates and the oblique Cartesian coordinate system $z, u \equiv x, v$ with reference to the angular region 1 of aperture γ ($0 < \varphi < \gamma$) with $0 < \gamma < \pi$ and delimited by faces a and o. In the figure, a second region is identified ($-\pi + \gamma < \varphi < 0$) delimited by faces b and o. The figure reports also the local-to-face Cartesian coordinate systems $Z_1 \equiv z, X_1, Y_1$ and $Z_2 \equiv z, X_2, Y_2$ respectively for face a of region 1 and face b of region 2. The local-to-face Cartesian coordinate systems are obtained from z, x, y Cartesian coordinate system by rotation, respectively for a positive γ and a negative $\pi - \gamma$. (b) The figure shows the new framework of the space divided into two angular regions useful for the study of wedge structures. The figure reports both the z, x, y Cartesian coordinates the oblique Cartesian coordinate system $z, u \equiv x, v$ where γ is the aperture angle of region 2. The figure reports also the local-to-face-b Cartesian coordinate system of region 2 $Z_{2'} \equiv z, X_{2'}, Y_{2'}$ that is obtained from z, x, y Cartesian coordinate system by rotation of an angle $-\gamma$. Finally in both figures we use also cylindrical coordinates (z, ρ, φ).

Starting from planar layered regions, we extend the theory to angular shaped regions of aperture γ as reported at Section 3 of [41] from isotropic to arbitrary linear media. With reference to region 1 of Fig. 1.(a), we derive from (2) the oblique transverse equations (19) using an oblique system of Cartesian axes $(z, u \equiv x, v)$:

$$x = u + v\cos\gamma,\ y = v\sin\gamma \tag{18}$$

$$-\frac{\partial}{\partial v}\boldsymbol{\psi_y}(u,v) = \boldsymbol{M}_\gamma(-j\alpha_o, \frac{\partial}{\partial u}) \cdot \boldsymbol{\psi_y}(u,v) \tag{19}$$

The application of Fourier transform along $u = x$ reduces (19) to

$$-\frac{d}{dv}\boldsymbol{\psi_y}(\eta,v) = \boldsymbol{M}_\gamma(-j\alpha_o, -j\eta) \cdot \boldsymbol{\psi_y}(\eta,v) \tag{20}$$

where $\boldsymbol{\psi_y}(u,v) \doteq \frac{1}{2\pi}\int_{-\infty}^{\infty} \boldsymbol{\psi_y}(\eta,v)e^{-j\eta u}d\eta$ and

$$\boldsymbol{M}_\gamma(-j\alpha_o, -j\eta) = \boldsymbol{M}_{\gamma o} - j\eta\boldsymbol{M}_{\gamma 1} - \eta^2\boldsymbol{M}_{\gamma 2} \tag{21}$$

$$\boldsymbol{M}_{\gamma o} = \boldsymbol{M}_{y o} \sin\gamma, \quad \boldsymbol{M}_{\gamma 1} = \boldsymbol{M}_{y 1} \sin\gamma - \boldsymbol{I}_t \cos\gamma, \quad \boldsymbol{M}_{\gamma 2} = \boldsymbol{M}_{y 2} \sin\gamma \tag{22}$$

Based on the link between $\boldsymbol{M}_\gamma$ and $\boldsymbol{M}_y$, we have that $\boldsymbol{M}_\gamma$ has same eigenvectors $\boldsymbol{u_i}$ of $\boldsymbol{M}_y$, and the following relationship between the eigenvalues $\lambda_{\gamma i}(\gamma)$ and λ_i

$$\lambda_{\gamma i}(\gamma) = j\eta\cos\gamma + \lambda_i \sin\gamma \ , \ i = 1..4 \tag{23}$$

resulting into the following "oblique" $v-$longitudinal propagation constants

$$m_i(\gamma) = -j\lambda_{\gamma i}(\gamma) = +\eta\cos\gamma + \xi_i \sin\gamma \ , \ i = 1,2 \tag{24}$$
$$m_i(\gamma) = +j\lambda_{\gamma i}(\gamma) = -\eta\cos\gamma + \xi_i \sin\gamma \ , \ i = 3,4 \tag{25}$$

in agreement with the relationship between λ_i and ξ_i, and with correlated progressive and regressive propagating interpretation along the longitudinal direction y and along the oblique "longitudinal" direction v (progressive/regressive $e^{\mp j m_i v}$). We note that the quantities $\boldsymbol{M}_\gamma(-j\alpha_o, -j\eta)$, $\lambda_{\gamma i}(\gamma)$ and $m_i(\gamma)$ depend on the geometrical parameter γ and on the spectral variable η.

With reference to region 1 of Fig. 1.(a) we obtain the functional equations with circuital interpretation as mathematical manipulation of the solution of the differential equation (19) using Laplace domain $\tilde{\boldsymbol{\psi}}_{\boldsymbol{y}}(\eta, v) \doteq \int_0^\infty e^{j\eta u} \boldsymbol{\psi_y}(u, v) du$:

$$-\frac{d}{dv}\tilde{\boldsymbol{\psi}}_{\boldsymbol{y}}(\eta, v) = \boldsymbol{M}_\gamma(-j\alpha_o, -j\eta) \cdot \tilde{\boldsymbol{\psi}}_{\boldsymbol{y}}(\eta, v) + \boldsymbol{\psi_{sa}}(v), \ v > 0 \tag{26}$$

$$\boldsymbol{\psi_{sa}}(v) = -\boldsymbol{M}_{\gamma 1} \cdot \boldsymbol{\psi_y}(0_+, v) + j\eta \ \boldsymbol{M}_{\gamma 2} \cdot \boldsymbol{\psi_y}(0_+, v) - \boldsymbol{M}_{\gamma 2} \cdot \frac{\partial}{\partial u}\boldsymbol{\psi_y}(u, v)\Big|_{u=0_+} \tag{27}$$

The benefit of using Laplace transform is correlated to incorporation of boundary conditions through initial conditions with the term $\boldsymbol{\psi_{sa}}(v)$. In (26)-(27) the condition $u = 0_+, v > 0$ imposes boundary conditions on the fields along face a of Fig.1.(a). The solution is performed by using the characteristic Green's function procedure [41] in terms of homogeneous and particular solutions yielding the representation

$$\tilde{\boldsymbol{\psi}}_{\boldsymbol{y}}(\eta, v) = \sum_{i=1}^{4} C_i e^{-\lambda_{\gamma i}(\gamma)\, v} \boldsymbol{u_i} - \sum_{i=1}^{2} \boldsymbol{u_i v_i} \cdot \int_0^v e^{-\lambda_{\gamma i}(\gamma)(v-v')} \boldsymbol{\psi_{sa}}(v') dv' + \sum_{i=3}^{4} \boldsymbol{u_i v_i} \cdot \int_v^\infty e^{-\lambda_{\gamma i}(\gamma)(v-v')} \boldsymbol{\psi_{sa}}(v') dv' \tag{28}$$

Now, considering asymptotic behavior of exponential functions in v for $v \to +\infty$ of (28), we need to have $C_3 = C_4 = 0$ and at the same times the first couple of integrals are null (since $Re[\lambda_{1,2}] > 0$, $Re[\lambda_{3,4}] < 0$, respectively related to progressive and regressive waves). For this reason setting $v = 0$ we get the spectral field representation along face o

$$\tilde{\boldsymbol{\psi}}_{\boldsymbol{o+}}(\eta) \doteq \tilde{\boldsymbol{\psi}}_{\boldsymbol{y}}(\eta, 0) = C_1 \boldsymbol{u_1} + C_2 \boldsymbol{u_2} + \sum_{i=3}^{4} \boldsymbol{u_i v_i} \cdot \int_0^\infty e^{-\lambda_{\gamma i}(\gamma)(v-v')} \boldsymbol{\psi_{sa}}(v') dv' \tag{29}$$

By weighting (29) with the reciprocal vectors $\boldsymbol{v_3}, \boldsymbol{v_4}$ of $\boldsymbol{M}_\gamma$, we get the functional equations

$$\boldsymbol{v_i} \cdot \tilde{\boldsymbol{\psi}}_{\boldsymbol{o+}}(\eta) = \boldsymbol{v_i} \cdot \tilde{\boldsymbol{\psi}}_{\boldsymbol{sa+}}(-m_i(\gamma)), \quad i = 3,4 \tag{30}$$

where we have used the definition of Laplace transform

$$\tilde{\boldsymbol{\psi}}_{\boldsymbol{sa+}}(-m_i(\gamma)) \doteq \int_0^\infty e^{-j m_i(\gamma) v} \boldsymbol{\psi_{sa}}(v) dv = \int_0^\infty e^{-j m_i(\gamma)\rho} \boldsymbol{\psi_{sa}}(\rho) d\rho \tag{31}$$

With reference to Fig.1.(a) and its caption, analyzing and expanding $\tilde{\boldsymbol{\psi}}_{\boldsymbol{sa}+}(-m_i(\gamma))$ in (30) using Maxwell's equations, we rephrase the functional equations for region 1 into

$$\boldsymbol{v_i}\cdot\tilde{\boldsymbol{\psi}}_{\boldsymbol{o}+}(\eta)=\boldsymbol{v_i}\cdot\boldsymbol{T}(\gamma)\cdot\tilde{\boldsymbol{\psi}}_{\boldsymbol{a}+}(-m_i(\gamma),\gamma),\quad i=3,4 \tag{32}$$

where $\tilde{\boldsymbol{\psi}}_{\boldsymbol{o}+}(\eta)$ is the η Laplace transform of tangent-to-face-o field components (i.e. at $\varphi=0$) in Cartesian (z,x,y) and cylindrical coordinates (z,ρ,φ) (omitting z coordinate for invariance)

$$\begin{aligned}\tilde{\boldsymbol{\psi}}_{\boldsymbol{o}+}(\eta)=&\int_0^\infty|E_z(x,0),E_x(x,0),H_z(x,0),H_x(x,0)|^t e^{j\eta x}dx\\&=\int_0^\infty|E_z(\rho,0),E_\rho(\rho,0),H_z(\rho,0),H_\rho(\rho,0)|^t e^{j\eta\rho}d\rho\end{aligned}, \tag{33}$$

$\tilde{\boldsymbol{\psi}}_{\boldsymbol{a}+}(-m_i(\gamma),\gamma)$ is the $-m_i(\gamma)$ Laplace transform of tangent-to-face-a field components (i.e. at $\varphi=\gamma$) in local-to-face-a Cartesian (z,X_1,Y_1) coordinates and global cylindrical coordinates (z,ρ,φ) (located at $\varphi=+\gamma$)

$$\begin{aligned}\tilde{\boldsymbol{\psi}}_{\boldsymbol{a}+}(-m_i(\gamma),\gamma)=&\int_0^\infty|E_z(X_1,0),E_{X_1}(X_1,0),H_z(X_1,0),H_{X_1}(X_1,0)|^t e^{-jm_i(\gamma)X_1}dx\\&=\int_0^\infty|E_z(\rho,\gamma),E_\rho(\rho,\gamma),H_z(\rho,\gamma),H_\rho(\rho,\gamma)|^t e^{-jm_i(\gamma)\rho}d\rho\end{aligned} \tag{34}$$

and

$$\boldsymbol{T}(\gamma)=\begin{pmatrix}\frac{\sin(\gamma)(\alpha_o\xi_{yy}+\zeta_{xy}\xi_{yy}\omega-\mu_{xy}\omega\epsilon_{yy})}{\omega(\mu_{yy}\epsilon_{yy}-\zeta_{yy}\xi_{yy})}+\cos(\gamma) & 0 & \frac{\sin(\gamma)(\alpha_o\mu_{yy}+\zeta_{xy}\mu_{yy}\omega-\zeta_{yy}\mu_{xy}\omega)}{\omega(\mu_{yy}\epsilon_{yy}-\zeta_{yy}\xi_{yy})} & 0\\ \frac{\sin(\gamma)(-\zeta_{zy}\xi_{yy}\omega+\eta\xi_{yy}+\mu_{zy}\omega\epsilon_{yy})}{\omega(\mu_{yy}\epsilon_{yy}-\zeta_{yy}\xi_{yy})} & 1 & \frac{\sin(\gamma)(\zeta_{yy}\mu_{zy}\omega-\zeta_{zy}\mu_{yy}\omega+\eta\mu_{yy})}{\omega(\mu_{yy}\epsilon_{yy}-\zeta_{yy}\xi_{yy})} & 0\\ \frac{\sin(\gamma)(-\alpha_o\epsilon_{yy}-\xi_{yy}\omega\epsilon_{xy}+\xi_{xy}\omega\epsilon_{yy})}{\omega(\mu_{yy}\epsilon_{yy}-\zeta_{yy}\xi_{yy})} & 0 & \cos(\gamma)-\frac{\sin(\gamma)(\alpha_o\zeta_{yy}-\zeta_{yy}\xi_{xy}\omega+\mu_{yy}\omega\epsilon_{xy})}{\omega(\mu_{yy}\epsilon_{yy}-\zeta_{yy}\xi_{yy})} & 0\\ \frac{\sin(\gamma)(\xi_{yy}\omega\epsilon_{zy}-\epsilon_{yy}(\eta+\xi_{zy}\omega))}{\omega(\mu_{yy}\epsilon_{yy}-\zeta_{yy}\xi_{yy})} & 0 & \frac{\sin(\gamma)(\mu_{yy}\omega\epsilon_{zy}-\zeta_{yy}(\eta+\xi_{zy}\omega))}{\omega(\mu_{yy}\epsilon\mathrm{yy}-\zeta_{yy}\xi_{yy})} & 1\end{pmatrix} \tag{35}$$

Note that (32) are functional equations that relate the Laplace transforms of combinations of field components on the boundaries of the angular region 1 of Fig.1.(a) , i.e. face o $u>0$, $v=0$ ($\varphi=0$) and face a $u=0$, $v>0$ ($\varphi=\gamma$). Furthermore, we observe that the angle γ is essential in determining the impact of anisotropies through $\boldsymbol{T}(\gamma)$.

Repeating the same procedure for region 2 of Fig. 1.(a), we obtain the functional equations as the solution of the differential equation (19) in Laplace domain using the left Laplace transform $\tilde{\boldsymbol{\psi}}_{\boldsymbol{y}}(\eta,v)\doteq\int_{-\infty}^{0}e^{j\eta\,u}\boldsymbol{\psi}_{\boldsymbol{y}}(u,v)du$:

$$-\frac{d}{dv}\tilde{\boldsymbol{\psi}}_{\boldsymbol{y}}(\eta,v)=\boldsymbol{M}_{\boldsymbol{\gamma}}(-j\alpha_o,-j\eta)\cdot\tilde{\boldsymbol{\psi}}_{\boldsymbol{y}}(\eta,v)+\boldsymbol{\psi}_{\boldsymbol{sb}}(v),\ v<0 \tag{36}$$

where $\boldsymbol{\psi}_{\boldsymbol{sb}}(v)$ has the same expression of $\boldsymbol{\psi}_{\boldsymbol{sa}}(v)$ (27) but with different support $v<0$ and it allows the incorporation of boundary conditions along face b ($u=0_+,v<0$). The application of characteristic Green's function procedure yields for region 2 of Fig. 1.(a) the expression (28), which is identical to the one of region 1 except for C_i and the source term $\boldsymbol{\psi}_{\boldsymbol{sb}}(v)$ that depend on local constitutive parameters and boundary conditions of region 2. Now, considering asymptotic behavior of exponential function in v for $v\to-\infty$, we need to have $C_1=C_2=0$ and at the same times the second couple of integrals are null. For this reason setting $v=0$ we get

$$\tilde{\boldsymbol{\psi}}_{\boldsymbol{o}+}(\eta)\doteq\tilde{\boldsymbol{\psi}}_{\boldsymbol{y}}(\eta,0)=C_3\boldsymbol{u_3}+C_4\boldsymbol{u_4}-\sum_{i=1}^{2}\boldsymbol{u_i}\boldsymbol{v_i}\cdot\int_0^\infty e^{-\lambda_i(\gamma)(v-v')}\boldsymbol{\psi}_{\boldsymbol{sb}}(v')dv' \tag{37}$$

By weighting (37) with the reciprocal vectors $\boldsymbol{v_1}, \boldsymbol{v_2}$ of $\boldsymbol{M}_\gamma$ we get the functional equations

$$\boldsymbol{v_i} \cdot \tilde{\boldsymbol{\psi}}_{\boldsymbol{o}+}(\eta) = -\boldsymbol{v_i} \cdot \tilde{\boldsymbol{\psi}}_{\boldsymbol{sb}+}(-m_i(\gamma)), \quad i = 1,2 \tag{38}$$

where we have used the definition of v left Laplace transform

$$\tilde{\boldsymbol{\psi}}_{\boldsymbol{sb}+}(-m_i(\gamma)) \doteq \int_{-\infty}^{0} e^{-jm_i(\gamma)v} \boldsymbol{\psi_{sb}}(v)dv = \int_{0}^{\infty} e^{-jm_i(\gamma)\rho} \boldsymbol{\psi_{sb}}(-\rho)d\rho \tag{39}$$

Note the differences and similarities between Laplace transformations (31) and (39) that yields same definition of $-m_i(\gamma)$ Laplace transform in ρ but applied to different quantities. Furthermore, the regularity properties of $-m_i(\gamma)$ Laplace transform are inherited from ξ_i ($Im[\xi_i] < 0$) according to (24)-(25).

With reference to Fig.1.(a) and its caption, analyzing and expanding $\tilde{\boldsymbol{\psi}}_{\boldsymbol{sb}+}(-m_i(\gamma))$ in (38), we rephrase the functional equations into

$$\boldsymbol{v_i} \cdot \tilde{\boldsymbol{\psi}}_{\boldsymbol{o}+}(\eta) = -\boldsymbol{v_i} \cdot \boldsymbol{T}(\gamma) \cdot \boldsymbol{P} \cdot \tilde{\boldsymbol{\psi}}_{\boldsymbol{b}+}(-m_i(\gamma), -\pi+\gamma), \quad i = 1,2 \tag{40}$$

In (40), $\boldsymbol{T}(\gamma)$ is the one reported at (35) for region 1, $\boldsymbol{P} = diag\{1,-1,1,-1\}$ is needed for $v = -X_2$ in region 2 with respect to $v = X_1$ in region 1 , $\tilde{\boldsymbol{\psi}}_{\boldsymbol{o}+}(\eta)$ is the η Laplace transform of tangent-to-face-o field components reported in (33) and $\tilde{\boldsymbol{\psi}}_{\boldsymbol{b}+}(-m_i(\gamma), -\pi+\gamma)$ is the $-m_i(\gamma)$ Laplace transform of tangent-to-face-b field components (i.e. at $\varphi = -\pi+\gamma$) in local-to-face-b Cartesian (z, X_2, Y_2) coordinates and global cylindrical coordinates (z, ρ, φ) of Fig. 1.(a)

$$\begin{aligned}\tilde{\boldsymbol{\psi}}_{\boldsymbol{b}+}(-m_i(\gamma), -\pi+\gamma) &= \int_0^\infty |E_z(X_2,0), E_{X_2}(X_2,0), H_z(X_2,0), H_{X_2}(X_2,0)|^t e^{-jm_i(\gamma)X_2}dx \\ &= \int_0^\infty |E_z(\rho,-\pi+\gamma), E_\rho(\rho,-\pi+\gamma), H_z(\rho,-\pi+\gamma), H_\rho(\rho,-\pi+\gamma)|^t e^{-jm_i(\gamma)\rho}d\rho\end{aligned} \tag{41}$$

While considering wedge scattering problem with symmetry with respect to x axis, in combination with region 1 of Fig.1.(a), we need to consider region 2′ of Fig.1.(b) where $\gamma \to \pi - \gamma$ with respect to region 2 of Fig.1.(a), i.e. for the same face a at $\varphi = \gamma$ we change orientation of face b from $\varphi = -\pi+\gamma$ to $\varphi = -\gamma$. The functional equations of region 2′ becomes

$$\boldsymbol{v_i} \cdot \tilde{\boldsymbol{\psi}}_{\boldsymbol{o}+}(\eta) = -\boldsymbol{v_i} \cdot \boldsymbol{T}(\pi-\gamma) \cdot \boldsymbol{P} \cdot \tilde{\boldsymbol{\psi}}_{\boldsymbol{b}+}(-m_i(\pi-\gamma), -\gamma), \quad i = 1,2 \tag{42}$$

where

$$\begin{aligned}\tilde{\boldsymbol{\psi}}_{\boldsymbol{b}+}(-m_i(\pi-\gamma), -\gamma) &= \int_0^\infty |E_z(X_2,0), E_{X_2}(X_2,0), H_z(X_2,0), H_{X_2}(X_2,0)|^t e^{-jm_i(\pi-\gamma)X_2}dx \\ &= \int_0^\infty |E_z(\rho,-\gamma), E_\rho(\rho,-\gamma), H_z(\rho,-\gamma), H_\rho(\rho,-\gamma)|^t e^{-jm_i(\pi-\gamma)\rho}d\rho\end{aligned} \tag{43}$$

which is the $-m_i(\pi-\gamma)$ Laplace transform of tangent-to-face-b field components (i.e. now at $\varphi = -\gamma$) in local-to-face-b Cartesian (z, X_2, Y_2) coordinates and global cylindrical coordinates (z, ρ, φ) of Fig. 1.(b). Note that in (42) we have assumed: region 2′ is homogeneous to region 1 yielding same u_i, v_i otherwise specific vectors would be needed. Eqs. (42) are functional equations that relate the Laplace transforms of combinations of field components on the boundaries of the angular region 2′ of Fig.1.(b) , i.e. face o $u > 0$, $v = 0$ ($\varphi = 0$) and face b $u = 0$, $v < 0$ ($\varphi = -\gamma$). In (42), note the new dependence of $\boldsymbol{T}(\cdot)$ (35) on $\pi - \gamma$, due to the effect of anisotropies while changing orientation of face b from $-\pi+\gamma$ to $-\gamma$. Furthermore, in case of symmetric media ($\lambda_{1,2} = -\lambda_{3,4}$) we have $m_{3,4}(\gamma) = m_{1,2}(\pi-\gamma)$, see (24)-(25).

In general, the system of functional equations (32), (42) allow the analysis of angular regions symmetric with respect to x axis that are at the base of the analysis of scattering problems constituted by impenetrable and penetrable wedges surrounded/made by arbitrary linear media. In the following, to investigate practical scattering problem, we impose boundary conditions at the faces of each angular region to the functional equations (32), (42), yielding a system of GWHEs.

3. From Functional Equations to GWHEs and their Regularized Integral Representations with Network Interpretation

Network representations of angular regions in isotropic media for electromagnetic scattering have been extensively studied in multiple spectral domains in [17] using algebraic and integral formalism. The proposed equations are effectively applied in several works to practical wedge scattering problems, see [15,16] and references therein. Furthermore network formalism has been effectively applied for complex canonical problems containing angular and layers regions in isotropic media, see for instance double wedge [37], flanged dielectric loaded waveguide [38], wedge over dielectric layer [36].

In arbitrary linear media, the system of functional equations (32), (42)

$$\begin{aligned} &\boldsymbol{v_i}\cdot\tilde{\boldsymbol{\psi}}_{\boldsymbol{o}+}(\eta)=\boldsymbol{v_i}\cdot\boldsymbol{T}(\gamma)\cdot\tilde{\boldsymbol{\psi}}_{\boldsymbol{a}+}(-m_i(\gamma),\gamma),\quad i=3,4\\ &\boldsymbol{v_i}\cdot\tilde{\boldsymbol{\psi}}_{\boldsymbol{o}+}(\eta)=-\boldsymbol{v_i}\cdot\boldsymbol{T}(\pi-\gamma)\cdot\boldsymbol{P}\cdot\tilde{\boldsymbol{\psi}}_{\boldsymbol{b}+}(-m_i(\pi-\gamma),-\gamma),\quad i=1,2\end{aligned} \tag{44}$$

constitutes two system of network relations that links respectively spectral field components in region 1 and region 2′ (Fig.1) via a sort of two port transmission relations in algebraic form. Looking at the first system in (44), we have two combinations of $\tilde{\boldsymbol{\psi}}_{\boldsymbol{o}+}(\eta)$ components (33) related to two combinations of $\tilde{\boldsymbol{\psi}}_{\boldsymbol{a}+}(-m_i(\gamma),\gamma)$ components (34), i.e., with reference to Fig. 1.(a), tangential field components of face o related to tangential field components of face a. A similar interpretation can be repeated for the second system in (44) about region 2 with field components defined at face o and b, respectively in $\tilde{\boldsymbol{\psi}}_{\boldsymbol{o}+}(\eta)$ (33) and $\tilde{\boldsymbol{\psi}}_{\boldsymbol{b}+}(-m_i(\pi-\gamma),-\gamma)$ (43).

We further note that in equations (44) the components of the face o and the face a,b are respectively functions of the spectral variables η and $-m_i(\cdot)$ that are related together via (24)-(25). We can reverse the role of the variables η and $-m_i(\cdot)$ in the arguments of the components of these faces. By this way we double the equations of the region 1, first line of (44) reported also in (45), with the equations of the second line (45) that relate the components of the face a (functions of the variable η) with the components of the face o (functions of $-m_i(\cdot)$). The second line of (45) is obtained defining region 1 as region 2′ (Fig. 1) after a clockwise rotation of an angle $+\gamma$, yielding the following complete set of equations for region 1:

$$\begin{aligned} &\boldsymbol{v_i}\cdot\tilde{\boldsymbol{\psi}}_{\boldsymbol{o}+}(\eta)=\boldsymbol{v_i}\cdot\boldsymbol{T}(\gamma)\cdot\tilde{\boldsymbol{\psi}}_{\boldsymbol{a}+}(-m_i(\gamma),\gamma),\quad i=3,4\\ &\boldsymbol{v_{iY_1}}\cdot\tilde{\boldsymbol{\psi}}_{\boldsymbol{a}+}(\eta)=-\boldsymbol{v_{iY_1}}\cdot\boldsymbol{T_{Y_1}}(\pi-\gamma)\cdot\boldsymbol{P}\cdot\tilde{\boldsymbol{\psi}}_{\boldsymbol{o}+}(-m_{iY_1}(\pi-\gamma),-\gamma),\quad i=1,2\end{aligned} \tag{45}$$

In the second couple of the equations (45) we have used subscript Y_1 to make reference to a rotated coordinated system (z,X_1,Y_1) with respect to (z,x,y), see region 1 in Fig. 2.(a) and related region 2′ in Fig. 2.(b). We note that the second couple of the equations in (45) are easily derived from studying a classical region 2′, see the second couple of the equations in (44), but with modified definitions of the quantities $\boldsymbol{v_{iY_1}}$,$\boldsymbol{T_{Y_1}}(\gamma)$, $m_{iY_1}(\gamma)$ (from $\lambda_{iY_1}(\gamma)$) because of their dependence on constitutive tensorial parameters $(\underline{\underline{\boldsymbol{\varepsilon}}},\underline{\underline{\boldsymbol{\mu}}},\underline{\underline{\boldsymbol{\xi}}},\underline{\underline{\boldsymbol{\zeta}}})$ of region 1 redefined in (z,X_1,Y_1) reference coordinate system, i.e. $(\underline{\underline{\boldsymbol{\varepsilon}}}_{Y_1},\underline{\underline{\boldsymbol{\mu}}}_{Y_1},\underline{\underline{\boldsymbol{\xi}}}_{Y_1},\underline{\underline{\boldsymbol{\zeta}}}_{Y_1})$, see for example

$$\underline{\underline{\boldsymbol{\varepsilon}}}_{Y_1}=\underline{\underline{\boldsymbol{R}}}_{Y_1}^{-1}\cdot\underline{\underline{\boldsymbol{\varepsilon}}}\cdot\underline{\underline{\boldsymbol{R}}}_{Y_1},\quad \underline{\underline{\boldsymbol{R}}}_{Y_1}=\begin{pmatrix}\cos(\gamma) & -\sin(\gamma) & 0\\ \sin(\gamma) & \cos(\gamma) & 0\\ 0 & 0 & 1\end{pmatrix} \tag{46}$$

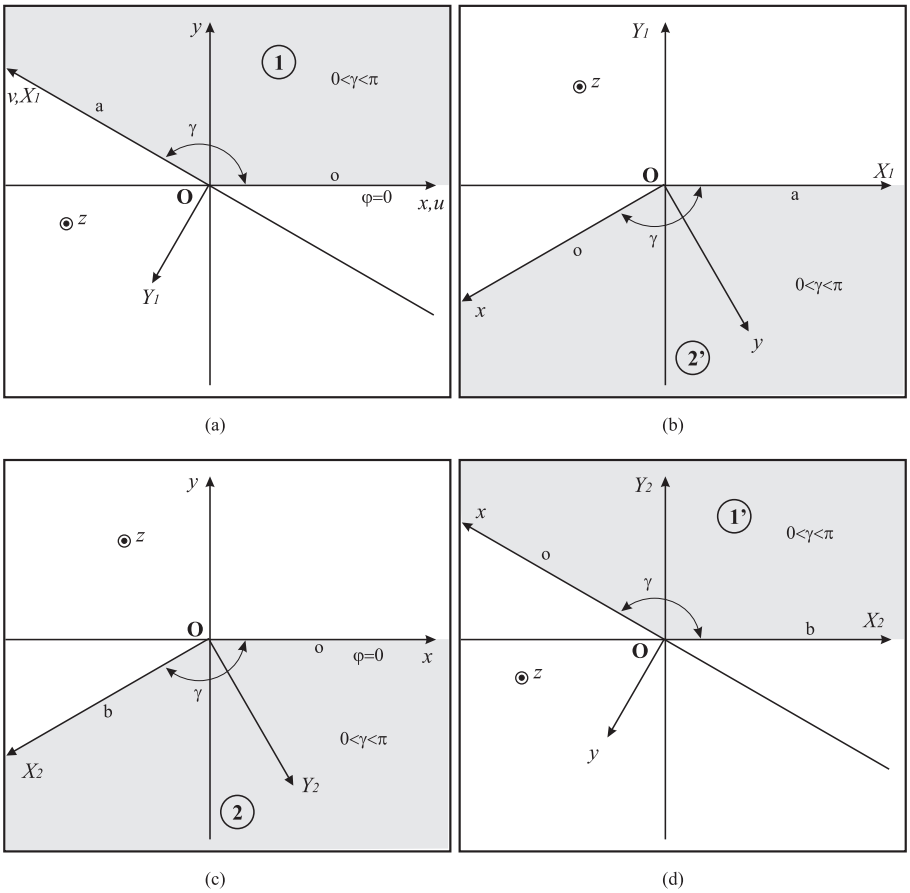

Figure 2. (a) Angular region 1 of aperture γ and delimited by faces a and o with original reference Cartesian coordinate system z, x, y. The figure reports also the local-to-face-a Cartesian coordinate systems $Z_1 \equiv z, X_1, Y_1$. (b) Angular region 1 after a clockwise rotation of an angle γ becomes a region 2′. The figure shows the reference systems of region 1 after rotation. (c) Angular region 2 of aperture γ and delimited by faces b and o with original reference Cartesian coordinate system z, x, y. The figure reports also the local-to-face-b Cartesian coordinate systems $Z_2 \equiv z, X_2, Y_2$. (d) Angular region 2 after a clockwise rotation of an angle γ becomes a region 1′. The figure shows the reference systems of region 2 after rotation.

due to a rotation of $+\gamma$.

The same rationale is applied to region 2 to double the equations of that region (second line of (44), reported also in (47)) by obtaining:

$$\begin{aligned} \boldsymbol{v}_{i\boldsymbol{Y}_2} \cdot \tilde{\boldsymbol{\psi}}_{\boldsymbol{b}+}(\eta) &= \boldsymbol{v}_{i\boldsymbol{Y}_2} \cdot \boldsymbol{T}_{\boldsymbol{Y}_2}(\gamma) \cdot \tilde{\boldsymbol{\psi}}_{\boldsymbol{o}+}(-m_{iY_2}(\gamma), \gamma), \quad i = 3, 4 \\ \boldsymbol{v}_{\boldsymbol{i}} \cdot \tilde{\boldsymbol{\psi}}_{\boldsymbol{o}+}(\eta) &= -\boldsymbol{v}_{\boldsymbol{i}} \cdot \boldsymbol{T}(\pi - \gamma) \cdot \boldsymbol{P} \cdot \tilde{\boldsymbol{\psi}}_{\boldsymbol{b}+}(-m_i(\pi - \gamma), -\gamma), \quad i = 1, 2 \end{aligned} \tag{47}$$

In the first couple of the equations (47) we have used subscript Y_2 to make reference to a rotated coordinated system (z, X_2, Y_2) with respect to (z, x, y), see region 2 Fig. 2.(c) and related region 1′ in Fig. 2.(d). We note that the first couple of the equations in (47) are easily derived from studying a classical region 1, see the first couple of the equations in (44), but with modified definitions of $\boldsymbol{v}_{i\boldsymbol{Y}_2}, \boldsymbol{T}_{\boldsymbol{Y}_2}(\gamma)$, $m_{iY_2}(\gamma)$ because of their dependence on constitutive parameters $(\underline{\underline{\boldsymbol{\varepsilon}}}, \underline{\underline{\boldsymbol{\mu}}}, \underline{\underline{\boldsymbol{\xi}}}, \underline{\underline{\boldsymbol{\zeta}}})$ redefined in (z, X_2, Y_2) reference coordinate system, i.e. $(\underline{\underline{\boldsymbol{\varepsilon}}}_{Y_2}, \underline{\underline{\boldsymbol{\mu}}}_{Y_2}, \underline{\underline{\boldsymbol{\xi}}}_{Y_2}, \underline{\underline{\boldsymbol{\zeta}}}_{Y_2})$, see for example

$$\underline{\underline{\boldsymbol{\varepsilon}}}_{Y_2} = \underline{\underline{\boldsymbol{R}}}_{Y_2}^{-1} \cdot \underline{\underline{\boldsymbol{\varepsilon}}} \cdot \underline{\underline{\boldsymbol{R}}}_{Y_2}, \quad \underline{\underline{\boldsymbol{R}}}_{Y_2} = \begin{pmatrix} \cos(\gamma) & \sin(\gamma) & 0 \\ -\sin(\gamma) & \cos(\gamma) & 0 \\ 0 & 0 & 1 \end{pmatrix} \tag{48}$$

due to a rotation of $-\gamma$.

The sets of equations (45) and (47) constitute a complete set of functional equations that describe respectively region 1 and 2 of Fig. 3 where in case of symmetric media (i.e. $\lambda_{1,2} = -\lambda_{3,4}$) we have $m_{3,4}(\gamma) = m_{1,2}(\pi - \gamma)$, see (24)-(25).

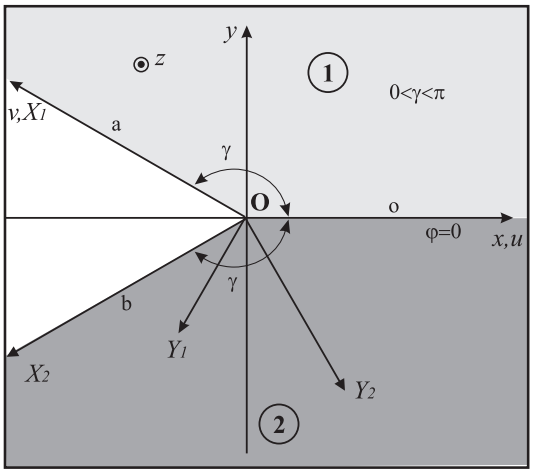

Figure 3. Two angular regions symmetric with respect to x axis of aperture angle γ that represent wedge problems immersed in arbitrary linear media, modeled by the complete sets of equations (45) and (47).

In isotropic media, it is always possible to introduce the angular complex plane w and the KL transform method [17] where functional equations become two port admittance relations of Norton type respectively in integral and algebraic form using a unique complex plane. In arbitrary linear media, the definition of such complex planes is not possible, however a novel method the resorts to the following Cauchy decomposition formula in $-m(\eta)$ plane is introduced. This is a fundamental tool that allows description of angular region problems in arbitrary linear media without introducing further complex planes except the initial Laplace transforms. In particular to get regularized integral equations from GWHEs, it is not necessary to map the GWHEs into CWHEs with suitable transformations before the application of Fredholm factorization (originally ideated and valid only for the CWHE). This revisited novel version of regularization procedure can be called *direct Fredholm factorization method*.

At the origin of this method we introduce the following generalized form of Cauchy decomposition formula in $-m(\eta)$ plane (i.e. one of $m_i(\cdot)$ that all depends on η and now we highlight the dependence on η for clarity) applied to an arbitrary $F_+(-m(\eta))$ as a generalization of standard Cauchy decomposition formula (i.e. the standard form is obtained by replacing $-m(\eta)$ simply with η):

$$F_+(-m(\eta)) = \frac{1}{2\pi j}\int_{-\infty}^{\infty}\frac{F_+(\eta')}{\eta' + m(\eta)}d\eta' + F_+^{n.s.}(-m(\eta)),\ \eta \in \mathbb{R} \tag{49}$$

where $F_+^{n.s.}(-m(\eta))$ is the non standard contribution of $F_+(-m(\eta))$ in $-m(\eta)$ plane. We observe that, in general assuming lossy media, $-m(\eta)$ is with positive imaginary part for $\eta \in \mathbb{R}$, i.e. located in the upper half-plane of complex plane η, thus the application of (49) on plus functions is justified (see for example Fig. 4 where we have assumed $k = 1 - 0.1j, \gamma = 0.7\pi$ that yields a $-m(t)$ for $t \in \mathbb{R}$ path from right to left because of $\gamma > \pi/2$, on the contrary for $\gamma < \pi/2$ we get a similar path located in the upper half plane but with opposite versus). We anticipate that the application of (49) to GWHEs with multiple propagation constants, i.e. multiple $m_i(\eta)$, is fundamental for developing a solution in η plane, as (49) transforms the GWHEs into integral equations in the unique complex plane η.

The complete sets of equations (45) for region 1 can be represented in the form

$$\begin{aligned}
A^E_{11}(\eta)E_{oz}(\eta)+A^E_{12}(\eta)E_{o\rho}(\eta)+A_{11}(\eta)H_{oz}(\eta)+A_{12}(\eta)H_{o\rho}(\eta) &= B^E_{11}(\eta)E_{az}(-m_3)+B^E_{12}(\eta)E_{a\rho}(-m_3)+B_{11}(\eta)H_{az}(-m_3)+B_{12}(\eta)H_{a\rho}(-m_3)\\
A^E_{21}(\eta)E_{oz}(\eta)+A^E_{22}(\eta)E_{o\rho}(\eta)+A_{21}(\eta)H_{oz}(\eta)+A_{22}(\eta)H_{o\rho}(\eta) &= B^E_{21}(\eta)E_{az}(-m_4)+B^E_{22}(\eta)E_{a\rho}(-m_4)+B_{21}(\eta)H_{az}(-m_4)+B_{22}(\eta)H_{a\rho}(-m_4)\\
A^E_{31}(\eta)E_{az}(\eta)+A^E_{32}(\eta)E_{a\rho}(\eta)+A_{31}(\eta)H_{az}(\eta)+A_{32}(\eta)H_{a\rho}(\eta) &= B^E_{31}(\eta)E_{oz}(-m_1)+B^E_{32}(\eta)E_{o\rho}(-m_1)+B_{31}(\eta)H_{oz}(-m_1)+B_{32}(\eta)H_{o\rho}(-m_1)\\
A^E_{41}(\eta)E_{az}(\eta)+A^E_{42}(\eta)E_{a\rho}(\eta)+A_{41}(\eta)H_{az}(\eta)+A_{42}(\eta)H_{a\rho}(\eta) &= B^E_{41}(\eta)E_{oz}(-m_2)+B^E_{42}(\eta)E_{o\rho}(-m_2)+B_{41}(\eta)H_{oz}(-m_2)+B_{42}(\eta)H_{o\rho}(-m_2)
\end{aligned} \tag{50}$$

where face o and face a spectral field components are related together[3].Moreover, the complete set of equations for region 2 (47) has a similar representation. The imposition of boundary conditions make these equations a well posed mathematical problem resulting in a GWHE system. In particular if the region is surrounded by something modeled by impenetrable impedance boundary conditions we establish relations among field components on the boundary faces. On the contrary, if the region is surrounded by penetrable regions, we establish continuity through tangent components to neighboring regions that provide further functional equations (coupled together). In any case the type of completed functional equations and constraints with boundary conditions remain always of the same form and are a well posed mathematical problem of GWHE type.

As a simple example to illustrate the procedure, let us consider a problem constituted by only region 1 with PEC boundary conditions filled by arbitrary linear media. In this case we get

$$\begin{aligned}
A_{11}(\eta)H_{oz}(\eta)+A_{12}(\eta)H_{o\rho}(\eta) &= B_{11}(\eta)H_{az}(-m_3)+B_{12}(\eta)H_{a\rho}(-m_3)\\
A_{21}(\eta)H_{oz}(\eta)+A_{22}(\eta)H_{o\rho}(\eta) &= B_{21}(\eta)H_{az}(-m_4)+B_{22}(\eta)H_{a\rho}(-m_4)\\
A_{31}(\eta)H_{az}(\eta)+A_{32}(\eta)H_{a\rho}(\eta) &= B_{31}(\eta)H_{oz}(-m_1)+B_{32}(\eta)H_{o\rho}(-m_1)\\
A_{41}(\eta)H_{az}(\eta)+A_{42}(\eta)H_{a\rho}(\eta) &= B_{41}(\eta)H_{oz}(-m_2)+B_{42}(\eta)H_{o\rho}(-m_2)
\end{aligned} \tag{51}$$

where in the LHS we have plus field unknowns in η and in the RHS we have minus field unknowns in $m_i()$. The apparent redundancy in (51) after imposition of boundary condition is exploited to get integral representations only in terms of the field components $H_{oz}(\eta)$, $H_{o\rho}(\eta)$, $H_{az}(\eta)$, $H_{a\rho}(\eta)$ in the unique complex plane η using (49). Furthermore the application of the novel version of Fredholm factorization method allows to get regularized integral equations. We assert that this procedure is applicable in general to GWHEs, not only for the specific problem represented in this simple example. The application of (49) to RHS of (51) yields

$$\begin{aligned}
A_{11}(\eta)H_{oz}(\eta)+A_{12}(\eta)H_{o\rho}(\eta) &= \tfrac{B_{11}(\eta)}{2\pi j}\int_{-\infty}^{\infty}\tfrac{H_{az}(\eta')}{\eta'+m_3}d\eta'+\tfrac{B_{12}(\eta)}{2\pi j}\int_{-\infty}^{\infty}\tfrac{H_{a\rho}(\eta')}{\eta'+m_3}d\eta'+H^{n.s}_{az}(-m_3)+H^{n.s}_{a\rho}(-m_3)\\
A_{21}(\eta)H_{oz}(\eta)+A_{22}(\eta)H_{o\rho}(\eta) &= \tfrac{B_{21}(\eta)}{2\pi j}\int_{-\infty}^{\infty}\tfrac{H_{az}(\eta')}{\eta'+m_4}d\eta'+\tfrac{B_{22}(\eta)}{2\pi j}\int_{-\infty}^{\infty}\tfrac{H_{a\rho}(\eta')}{\eta'+m_4}d\eta'+H^{n.s}_{az}(-m_4)+H^{n.s}_{a\rho}(-m_4)\\
A_{31}(\eta)H_{az}(\eta)+A_{32}(\eta)H_{a\rho}(\eta) &= \tfrac{B_{31}(\eta)}{2\pi j}\int_{-\infty}^{\infty}\tfrac{H_{oz}(\eta')}{\eta'+m_1}d\eta'+\tfrac{B_{32}(\eta)}{2\pi j}\int_{-\infty}^{\infty}\tfrac{H_{o\rho}(\eta')}{\eta'+m_1}d\eta'+H^{n.s}_{oz}(-m_1)+H^{n.s}_{o\rho}(-m_1)\\
A_{41}(\eta)H_{az}(\eta)+A_{42}(\eta)H_{a\rho}(\eta) &= \tfrac{B_{41}(\eta)}{2\pi j}\int_{-\infty}^{\infty}\tfrac{H_{az}(\eta')}{\eta'+m_2}d\eta'+\tfrac{B_{42}(\eta)}{2\pi j}\int_{-\infty}^{\infty}\tfrac{H_{a\rho}(\eta')}{\eta'+m_2}d\eta'+H^{n.s}_{oz}(-m_2)+H^{n.s}_{o\rho}(-m_2)
\end{aligned} \tag{52}$$

recalling that all occurrences of m_i are functions of η, i.e. $m_i(\eta)$. Integral equations (52) are of singular type, for this reason we resort to Fredholm factorization method to get regularized expressions. The procedure consists on γ_{1t} Cauchy *smile* contour integration [19],[15] on both side of each equation and consequent mathematical elaboration. Focusing

[3] Throughout the paper we assume in spectral equations the notation with two subscripts for the spectral field: the first subscript is related to the considered face (o, a, b) and the second to the field component (z, x, y).

the attention on the LHS for each term of each equation (52) we have, using dummy subscripts, the regularized expression

$$\begin{aligned}\frac{1}{2\pi j}\int_{\gamma_{1t}}\frac{A(t)H_+(t)}{t-\eta}dt &= \frac{1}{2\pi j}\int_{\gamma_{1t}}\frac{(A(t)-A(\eta))H_+(t)}{t-\eta}dt+\frac{A(\eta)}{2\pi j}\int_{\gamma_{1t}}\frac{H_+(t)}{t-\eta}dt\\ &= \frac{1}{2\pi j}\int_{-\infty}^{\infty}\frac{(A(t)-A(\eta))H_+(t)}{t-\eta}dt+A(\eta)H_+(\eta)-A(\eta)H_+^{n.s}(\eta)\end{aligned} \tag{53}$$

Focusing the attention on the RHS for each term of each equation (52) we have, using dummy subscripts and going back also to representation (51), the regularized expression

$$\begin{aligned}&\frac{1}{2\pi j}\int_{\gamma_{1t}}\frac{B(t)H_+(-m(t))}{t-\eta}dt=\frac{1}{2\pi j}\int_{\gamma_{1t}}\frac{(B(t)-B(\eta))H_+(-m(t))}{t-\eta}dt+\frac{B(\eta)}{2\pi j}\int_{\gamma_{1t}}\frac{H_+(-m(t))}{t-\eta}dt\\ &=\frac{1}{(2\pi j)^2}\int_{-\infty}^{\infty}\int_{-\infty}^{\infty}\frac{(B(t)-B(\eta))H_+(\eta')}{(t-\eta)(\eta'+m(t))}dt\,d\eta'+\frac{B(\eta)}{(2\pi j)^2}\int_{-\infty}^{\infty}\int_{\gamma_{1t}}\frac{1}{(t-\eta)(\eta'+m(t))}dtH_+(\eta')d\eta'+n.s.\,terms\end{aligned} \tag{54}$$

Given the expressions of $m_i(\eta)$ (24)-(25) with $Im[m_i(t)]<0$ in lossy media (Fig. 4.), (54) requires the computation of

$$M_e(\eta,\eta')=\int_{\gamma_{1t}}\frac{1}{(t-\eta)(\eta'+m(t))}dt \tag{55}$$

that can be performed either numerically or analytically paying attention to the branch cuts of $m(t)$. Furthermore in (54) we also need to consider n.s. singularities related to the field.

The validity of the estimation of $M_e(\eta,\eta')$ extends to complex values of η' as long as η' does not cross the singularity line determined by $-m(t)$ for $t\in\mathbb{R}$, as shown in Fig. 4.

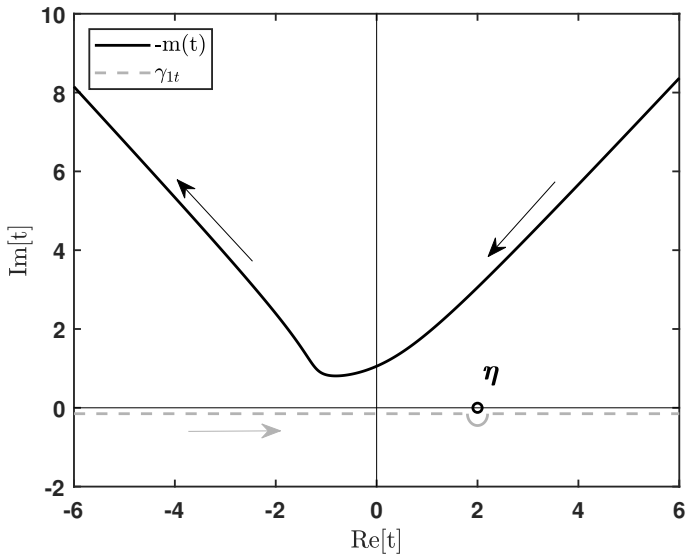

Figure 4. Cauchy *smile* contour integration line γ_{1t} and example of $-m(t)$ line for $t\in\mathbb{R}$, $k=1-0.1j,\gamma=0.7\pi$ (If $\gamma<\pi/2$ the behavior of $-m(t)$ is with similar direction but opposite versus. To intuitively understand this property in isotropic medium, use m definition in w plane and apply the formula for aperture angle that are supplementary.)

The expressions (53), (54) are regularized integral terms since their kernels are compact, moreover, they respectively include n.s. terms of field components in η and $-m_i$. The detailed proof of this assertion is to be performed for specific problems. However, while numerically implementing the method, we observe that one of the main difficulties resides in the correct estimation of kernel functions $A(\eta),B(\eta)$ for the presence of multivalued functions that need particular attention in their definition and calculation.

For simplicity and compactness of discussion we will examine the properties of integral equations in the simple case of a PEC wedge immersed in an isotropic medium in following section 5.2. Eq. (51) yields a 4x4 system of Fredholm integral equations of second kind by utilizing (52), (53), and (54). This system is expressed in terms of $H_{oz}(\eta)$, $H_{o\rho}(\eta)$, $H_{az}(\eta)$, $H_{a\rho}(\eta)$. It is important to highlight that the system only depends on the spectral variable η, ensuring that functions do not rely on m_i outside of the integration sign. This property is fundamental to avoid analysis of unknowns defined in different complex planes (η and multiple m_i) that are correlated through cumbersome improper sheet properties.

4. Asymptotic Estimation of Field in the Angular Region

Once the spectra at the faces of the angular region is obtained we can estimate the asymptotic behaviour of far field inside the angular region.

Going back to the solution of (26) in Section 2 for region 1 reported at (28), we have

$$\tilde{\boldsymbol{\psi}}_{\boldsymbol{y}}(\eta, v) = \sum_{i=1}^{2} C_i e^{-\lambda_{\gamma i}(\gamma)\, v} \boldsymbol{u_i} + \sum_{i=3}^{4} \boldsymbol{u_i v_i} \cdot \int_{v}^{\infty} e^{-\lambda_{\gamma i}(\gamma)(v-v')} \boldsymbol{\psi_{sa}}(v') dv', \; v > 0 \tag{56}$$

From the homogeneous portion of solution in (56) we get the definitions of arbitrary coefficient in terms of field components at $v = 0$ (face o):

$$\boldsymbol{v_i} \cdot \tilde{\boldsymbol{\psi}}_{\boldsymbol{y}}(\eta, 0) = C_i, \; i = 1, 2 \tag{57}$$

The particular integrals in (56) are terms related to face a via $\boldsymbol{\psi_{sa}}(v)$. Due to linearity of the problem we apply superposition principle and we can interpret (56) as the result of an equivalent theorem where $\tilde{\boldsymbol{\psi}}_{\boldsymbol{y}}(\eta, v)$ is represented through equivalent sources at face o and a. Similarly the spectral field in region 1 can be considered as result of the analysis of a rotated region 2′, Fig. 2.(b) in Section 3, yielding

$$-\frac{d}{dv}\tilde{\boldsymbol{\psi}}_{\boldsymbol{Y_1}}(\eta, v) = \boldsymbol{M_{\pi-\gamma}}(-j\alpha_o, -j\eta) \cdot \tilde{\boldsymbol{\psi}}_{\boldsymbol{Y_1}}(\eta, v) + \boldsymbol{\psi_{so}}(v), \; v < 0 \tag{58}$$

where we note $\gamma \to \pi - \gamma$ that it will impact on all terms of the solution as already reported in in Section 3: $\boldsymbol{u_{iY_1}}$, $\boldsymbol{v_{iY_1}}$, λ_{iY_1}, m_{iY_1} and field components. The solution takes the form

$$\tilde{\boldsymbol{\psi}}_{\boldsymbol{Y1}}(\eta, v) = \sum_{i=3}^{4} C_i e^{-\lambda_{\gamma i Y_1}(\pi-\gamma)\, v} \boldsymbol{u_{iY_1}} - \sum_{i=1}^{2} \boldsymbol{u_{iY_1} v_{iY_1}} \cdot \int_{v}^{\infty} e^{-\lambda_{\gamma i Y_1}(\pi-\gamma)(v-v')} \boldsymbol{\psi_{so}}(v') dv', \; v < 0 \tag{59}$$

where now $v = -x$ of Fig. 2.(b) different from $v = X_1$ of Fig. 2.(a). From the homogeneous portion of solution in (59) we get the definitions of arbitrary coefficient in terms of field components at $v = 0$ (face a):

$$\boldsymbol{v_{iY_1}} \cdot \tilde{\boldsymbol{\psi}}_{\boldsymbol{Y1}}(\eta, 0) = C_i, \; i = 3, 4 \tag{60}$$

The particular integrals in (59) are terms related to face o via $\boldsymbol{\psi_{so}}(v)$. Due to linearity of the problem we again apply superposition principle and we can interpret (59) as the result of an equivalent theorem where $\tilde{\boldsymbol{\psi}}_{\boldsymbol{Y1}}(\eta, v)$ is represented through equivalent sources at face a and o.

Using superposition principle and considering only homogeneous portions of (56) and (59) we can represent the complete field without the particular integrals. Each contribution originated from (56) and (59) is a spectral component that can be Fourier/Laplace inversely transformed in the physical domain (u, v) and they represent respectively the fields from equivalent currents distributed in half-planes (respectively face o and face a). The application of asymptotic representation of fields for each component in a unique global system of cylindrical coordinate provides the estimation of field in terms of classical GTD for the

angular region 1 but as superposition of GTD for two half-planes (face o and face a), like in Kirchhoff representations. This procedure will be detailed examined in the practical examples reported in the following sections and it is a fundamental tool to estimate GTD directly in Fourier/Laplace domain for angular region filled by arbitrarily linear media where GTD in w plane is not available (as commonly done in isotropic angular region). Indeed the computation of GTD for an angular region filled by arbitrarily linear media is here proposed by resorting to the computation of GTD in two half-plane problems.

An alternative way to obtain far field is based on the computation of spectral field for any azimuthal direction φ, by splitting the angular region into two subregions at any observation angle φ (subregion A $0 < \varphi' < \varphi$ and subregion B $\varphi < \varphi' < \gamma$). Once obtained face spectra at $\varphi = 0, \gamma$ for the entire angular region as proposed in the previous sections, we then relate the spectra at φ to the ones of the two faces by using the functional equations of the two subregions. These φ-parametric spectral representations of field spectra allow asymptotic evaluation of far field at any φ. We observe that the functional equations are written in terms of continuous field components at the boundary faces of the angular region, see section 4. This property can be interpreted as *a novel and original form of electromagnetic equivalence theorem in spectral domain in the context of angular region problems filled by an arbitrary linear medium.*

5. Validation of the Novel Regularization Procedure with a Simple Example: Direct Fredholm Factorization applied to the PEC Wedge in Isotropic Region

In order to validate the procedure from a mathematical point of view, let us first demonstrate efficacy for the simple case of a PEC angular region 1 (Fig. 2.(a),(b)) filled by an isotropic medium where closed form WH solution is available. We have for region 1 from

$$m = m_i(\pi - \gamma) = m_{i+2}(\gamma) = -\eta\cos\gamma + \xi\sin\gamma\ ,\ i = 1,2;\ \xi = \sqrt{k^2 - \alpha_o^2 - \eta^2} \tag{61}$$

$$\boldsymbol{u_1} = \begin{vmatrix} \frac{\tau_o^2}{\omega\,\varepsilon\,\xi} \\ -\frac{\alpha_o\eta}{\omega\,\varepsilon\,\xi} \\ 0 \\ 1 \end{vmatrix},\ \boldsymbol{u_2} = \begin{vmatrix} \frac{\alpha_o\eta}{\omega\,\varepsilon\,\xi} \\ -\frac{(\xi^2+\alpha_o^2)}{\omega\,\varepsilon\,\xi} \\ 1 \\ 0 \end{vmatrix},\ \boldsymbol{u_3} = \begin{vmatrix} -\frac{\tau_o^2}{\omega\,\varepsilon\,\xi} \\ \frac{\alpha_o\eta}{\omega\,\varepsilon\,\xi} \\ 0 \\ 1 \end{vmatrix},\ \boldsymbol{u_4} = \begin{vmatrix} -\frac{\alpha_o\eta}{\omega\,\varepsilon\,\xi} \\ \frac{(\xi^2+\alpha_o^2)}{\omega\,\varepsilon\,\xi} \\ 1 \\ 0 \end{vmatrix} \tag{62}$$

$$\begin{aligned} \boldsymbol{v_1} &= \begin{vmatrix} \frac{\xi^2+\alpha_o^2}{2\omega\,\mu\,\xi} & \frac{\alpha_0\eta}{2\omega\,\mu\,\xi} & 0 & \frac{1}{2} \end{vmatrix}, \boldsymbol{v_2} = \begin{vmatrix} -\frac{\alpha_0\eta}{2\omega\,\mu\,\xi} & -\frac{k^2-\alpha_o^2}{2\omega\,\mu\,\xi} & \frac{1}{2} & 0 \end{vmatrix} \\ \boldsymbol{v_3} &= \begin{vmatrix} -\frac{\xi^2+\alpha_o^2}{2\omega\,\mu\,\xi} & -\frac{\alpha_0\eta}{2\omega\,\mu\,\xi} & 0 & \frac{1}{2} \end{vmatrix}, \boldsymbol{v_4} = \begin{vmatrix} \frac{\alpha_0\eta}{2\omega\,\mu\,\xi} & \frac{k_o^2-\alpha_o^2}{2\omega\,\mu\,\xi} & \frac{1}{2} & 0 \end{vmatrix} \end{aligned} \tag{63}$$

the following functional equations [41] (first two equations in (45)):

$$\begin{aligned} &-\alpha_o\eta E_{o\rho}(\eta) + (\eta^2 - k^2)E_{oz}(\eta) + k\xi Z_o H_{o\rho}(\eta) \\ &= -\alpha_o\eta E_{a\rho}(-m) - [\eta\xi\sin(\gamma) + \cos(\gamma)(k^2 - \eta^2)]E_{az}(-m) \\ &+k\xi Z_o H_{a\rho}(-m) - \sin(\gamma)\alpha_o k Z_o H_{az}(-m) \end{aligned} \tag{64}$$

$$\begin{aligned} &(k^2 - \alpha_o^2)E_{o\rho}(\eta) + \alpha_o\eta E_{oz}(\eta) + k\xi Z_o H_{oz}(\eta) \\ &= (k^2 - \alpha_o^2)E_{a\rho}(-m) + \alpha_o[\cos(\gamma)\eta - \sin(\gamma)\xi]E_{az}(-m) \\ &+kZ_o[\sin(\gamma)\eta + \cos(\gamma)\xi]H_{az}(-m) \end{aligned} \tag{65}$$

At normal incidence ($\alpha_o = 0$) we get

$$-\xi E_{oz}(\eta) + kZ_o H_{o\rho}(\eta) = -[\eta\sin(\gamma) + \xi\cos(\gamma)]E_{az}(-m) + kZ_o H_{a\rho}(-m) \tag{66}$$

$$kE_{o\rho}(\eta) + \xi Z_o H_{oz}(\eta) = kE_{a\rho}(-m) + Z_o[\eta\sin(\gamma) + \xi\cos(\gamma)]H_{az}(-m) \tag{67}$$

where we notice decoupling of equations (66)-(67) respectively for E_z and H_z polarization. The imposition of PEC boundary on functional equations (66)-(67) condition yields the GWHEs

$$H_{o\rho}(\eta) = H_{a\rho}(-m) \tag{68}$$

$$\xi H_{oz}(\eta) = [\eta \sin(\gamma) + \xi \cos(\gamma)] H_{az}(-m) \tag{69}$$

with plus/minus filed unknowns respectively in η, m. We notice that the regularity properties of the problem depends on the multi-valued function $\xi = \sqrt{k^2 - \eta^2}$ (due to physical reason) [15] that defines proper and improper sheets of η plane.

5.1. Classical Solution of the GWHEs of the problem in Different Complex Planes

In order to illustrate and validate in the following subsection the new direct Fredholm factorization procedure of Section 3, in this subsection we present the classical WH solution of (68) and (69) obtained in closed form [15] with the help of: a specialized mapping, the factorization and the decomposition with the extraction of source terms such as Geometrical Optics (GO) fields for plane wave illumination. We also clarify in this subsection important properties related to different complex planes (including angular complex plane w) where the problem and the solutions are represented.

The specialized mapping is

$$\eta = -k \cos\left(\frac{\gamma}{\pi} \arccos\left(-\frac{\bar{\eta}}{k}\right)\right) \tag{70}$$

introduced for the first time in [11] and extensively used in isotropic wedge scattering problems as reported in [15]-[16]. The mapping transforms plus unknowns in η plane and minus unknowns in m plane (61) into respectively plus and minus unknowns in $\bar{\eta}$ plane, yielding Classical Wiener-Hopf Equations in the new complex plane $\bar{\eta}$:

$$H_{o\rho+}(\bar{\eta}) = H_{a\rho+}(-\bar{\eta}) \tag{71}$$

$$\xi H_{oz+}(\bar{\eta}) = [\eta \sin(\gamma) + \xi \cos(\gamma)] H_{az+}(-\bar{\eta}) \tag{72}$$

where ξ and η becomes functions of $\bar{\eta}$ and

$$m = k \cos\left(\frac{\gamma}{\pi} \arccos\left(-\frac{\bar{\eta}}{k}\right) + \gamma\right) \tag{73}$$

From this point, the solution proceeds as for CWHEs thus with factorization, decomposition and application fo Liouville's Theorem, considering plane wave illumination at E_z and H_z polarization respectively with incident waves:

$$E_z^i(\rho,\varphi) = E_o e^{jk\rho\cos(\varphi-\varphi_o)},\ H_\rho^i(\rho,\varphi) = -\frac{1}{j\omega\mu\rho}\frac{\partial E_z^i(\rho,\varphi)}{\partial\varphi} = \frac{k}{\omega\,\mu}\sin(\varphi-\varphi_o)e^{jk\rho\cos(\varphi-\varphi_o)}E_o \tag{74}$$

$$H_z^i(\rho,\varphi) = H_o e^{jk\rho\cos(\varphi-\varphi_o)},\ E_\rho^i(\rho,\varphi) = \frac{1}{j\omega\varepsilon\rho}\frac{\partial H_z^i(\rho,\varphi)}{\partial\varphi} = -\frac{k}{\omega\varepsilon}\sin(\varphi-\varphi_o)e^{jk\rho\cos(\varphi-\varphi_o)}H_o \tag{75}$$

Due to PEC boundary conditions, we obtain the following GO source terms tangential respectively to face a and o of angular region 1

$$H_x^{GO}(\rho,0) = -2\frac{E_o}{Z_o}\sin\varphi_o e^{jk\rho\cos\varphi_o},\ H_\rho^{GO}(\rho,\gamma) = 2\frac{E_o}{Z_o}\sin(\gamma-\varphi_o)e^{jk\rho\cos(\gamma-\varphi_o)} \tag{76}$$

$$H_z^{GO}(\rho,0) = 2H_o e^{jk\rho\cos(\varphi_o)},\ H_z^{GO}(\rho,\gamma) = 2H_o e^{jk\rho\cos(\gamma-\varphi_o)} \tag{77}$$

that in spectral domain, according to Laplace transforms (33) and (34), become

$$H_{o\rho}^{GO}(\eta) = \frac{-2jE_o \sin\varphi_o}{Z_o(\eta-\eta_o)},\ H_{a\rho}^{GO}(-m) = \frac{-2jE_o \sin(\gamma-\varphi_o)}{Z_o(m-m_o)} \tag{78}$$

$$H_{oz}^{GO}(\eta) = \frac{2jH_o}{\eta-\eta_o},\ H_{az}^{GO}(-m) = \frac{-2jH_o}{m-m_o} \tag{79}$$

with $\eta_o = -k\cos\varphi_o$, $m_o = k\cos(\gamma-\varphi_o)$. In $\bar{\eta}$ plane (70), the pole η_o is mapped into $\bar{\eta}_o = -k\cos(-\frac{\pi}{\gamma}\varphi_o)$. In the following, we assume $\varphi_o < \gamma/2$ to locate $\bar{\eta}_o$ in the upper half-plane of complex plane $\bar{\eta}$ yileding non-standard plus unknowns; generalization is straightforward yielding an $\bar{\eta}_o$ in the $\bar{\eta}$-lower half-plane while $\gamma/2 < \varphi_o < \gamma$.

Focusing the attention on E_z polarization, due to the simplicity of equation (71), we observe the absence of need of factorization, thus we perform decomposition to highlight non-standard contribution in the plus unknown $H_{o\rho+}(\bar{\eta})$ constituted of $H_{o\rho}^{GO}(\eta) = R/(\eta-\eta_o)$ (78) to be mapped into $\bar{\eta}$ plane (70) yielding $H_{o\rho}^{GO}(\bar{\eta}) = T/(\eta-\eta_o)$. We obtain:

$$H_{o\rho+}(\bar{\eta}) - \frac{T}{\bar{\eta}-\bar{\eta}_o} = H_{a\rho+}(-\bar{\eta}) - \frac{T}{\bar{\eta}-\bar{\eta}_o} \tag{80}$$

with

$$T = R\left.\frac{d\bar{\eta}}{d\eta}\right|_{\eta_o} = -2j\frac{\pi}{\gamma}\frac{E_o}{Z_o}\sin\frac{\pi}{\gamma}\varphi_o,\ R = \frac{-2jE_o\sin\varphi_o}{Z_o},\ \left.\frac{d\bar{\eta}}{d\eta}\right|_{\eta_o} = \frac{\pi}{\gamma}\frac{\sin\frac{\pi}{\gamma}\varphi_o}{\sin\varphi_o} \tag{81}$$

Due to regularity and asymptotic behavior of LHS and RHS of (80), applying Liouville's Theorem, (80) is equal to zero, thus we get simple closed form solutions:

$$H_{o\rho+}(\bar{\eta}) = \frac{T}{\bar{\eta}-\bar{\eta}_o},\quad H_{a\rho+}(\bar{\eta}) = -\frac{T}{\bar{\eta}+\bar{\eta}_o} \tag{82}$$

Solutions (82) can be mapped into η plane using the inverse mapping of (70)

$$\bar{\eta} = -k\cos\left(\frac{\pi}{\gamma}\arccos\left(-\frac{\eta}{k}\right)\right) \tag{83}$$

We recall that the regularity properties of the problem (68)-(69) in η plane depends on the multi-valued function $\xi = \sqrt{k^2-\eta^2}$ (due to physical reason) and now, after the application of the mapping (70), on the multi-valued function $\kappa = \sqrt{k^2-\bar{\eta}^2}$ in $\bar{\eta}$ plane through log representation of $\arccos(-\bar{\eta}/k)$, see section 3.4 of [15]. Contrary to (70), the transformation (83) requires particular attention since it maps $\bar{\eta}$ into η for $0 < \gamma < \pi$ without covering the entire proper sheet of η plane defined by ξ function. For this reason, portion of η proper sheet falls into improper sheet of $\bar{\eta}$ plane and, since the closed form solution is obtained in $\bar{\eta}$ plane, this solution must be considered correct (not offending) only in the proper sheet of $\bar{\eta}$ also after applying the transformation (83). To easily control proper/improper sheets of η and $\bar{\eta}$ plane we can resort to their visualization in complex plane w ($\eta = -k\cos w$, thus $\bar{\eta} = -k\cos\left(\frac{\pi}{\gamma}w\right)$ and $m = k\cos(w+\gamma)$). The w plane shows the proper sheets of both planes $(\eta, \bar{\eta})$ in a unique plane. In particular, for real w the proper segments originated from η and $\bar{\eta}$ (respectively related to ξ and κ) are $-\pi < w < 0$ and $-\gamma < w < 0$, see section 3.4 of [15]. This means that the closed form solution obtained in the proper sheet of $\bar{\eta}$ is not valid in the entire proper sheet of η plane but only in a portion due to the properties of (83).

Let us now consider the CWHE of H_z polarization (72):

$$G(\bar{\eta})H_{oz+}(\bar{\eta}) = H_{az+}(-\bar{\eta}),\ G(\bar{\eta}) = \xi/n \tag{84}$$

with $n = -\eta \sin(\gamma) - \xi \cos(\gamma) = \sqrt{k^2 - m^2}$. According to [40], we have the factorization

$$G_-(\bar{\eta}) = \frac{G(\bar{\eta})}{G_+(\bar{\eta})},\ G_+(\bar{\eta}) = \frac{\xi}{\xi_- n_+},\ \xi_- = \sqrt{k - \bar{\eta}},\ n_+ = \sqrt{k + \bar{\eta}} \tag{85}$$

Confirming the same assumption $\varphi_o < \gamma/2$ for simplicity, $\bar{\eta}_o$ is located in the $\bar{\eta}$ upper half-plane, yielding a non standard plus unknown $H_{oz+}(\bar{\eta})$ constituted by the source non standard component $H_{oz}^{GO}(\eta) = R_H/(\eta - \eta_o)$ (79) that in $\bar{\eta}$ plane becomes:

$$H_{oz}^{GO}(\bar{\eta}) = \frac{T_H}{\bar{\eta} - \bar{\eta}_o},\ T_H = R_H \frac{d\bar{\eta}}{d\eta}\bigg|_{\eta_o} = 2jH_o \frac{\pi}{\gamma} \frac{\sin \frac{\pi}{\gamma}\varphi_o}{\sin \varphi_o},\ R_H = 2jH_o \tag{86}$$

Applying factorization and decomposition to (84) we get

$$G_+(\bar{\eta}) H_{oz+}(\bar{\eta}) - G_+(\bar{\eta}_o) H_{oz}^{GO}(\bar{\eta}) = G_-^{-1}(\bar{\eta}) H_{az+}(-\bar{\eta}) - G_+(\bar{\eta}_o) H_{oz}^{GO}(\bar{\eta}) \tag{87}$$

Due to regularity and asymptotic behavior of LHS and RHS of (87), applying Liouville's Theorem, (87) is equal to zero, thus we get simple closed form solutions:

$$H_{oz+}(\bar{\eta}) = G_+^{-1}(\bar{\eta}) G_+(\bar{\eta}_o) H_{oz}^{GO}(\bar{\eta}),\ H_{az+}(-\bar{\eta}) = G_-(\bar{\eta}) G_+(\bar{\eta}_o) H_{oz}^{GO}(\bar{\eta}) \tag{88}$$

Again the closed form solutions (88) at H_z polarization obtained in the proper sheet of $\bar{\eta}$ plane can be mapped into η plane using the inverse mapping (83), but we need to consider these solutions valid only for η values belonging to the proper sheet of $\bar{\eta}$ plane. Moreover this property can be ascertained by checking that (68)-(69) (provided the solutions in $\bar{\eta}$) are enforced only for η values belonging to the proper sheet of $\bar{\eta}$ plane.

In order to obtain solutions valid in the entire proper sheet of η plane or beyond (i.e. also in the improper sheet) we need to resort to analytical continuation technique that, in case of unique propagation constant as in isotropic media problem, can be implemented via representation of GWHEs (e.g (68)-(69)) into the w complex plane as difference equations, see examples in [15]-[16]. Another option is to describe the problem with unique propagation constant directly in w plane where the concept of proper and improper sheets of η and $\bar{\eta}$ planes are expanded periodically into w plane with an alternative vision of Riemann sheets. In this case the closed form solutions corresponding to (88) are (89) are valid in the entire w plane as opposed to approximate solutions obtained with line numerical integration located in a particular sheet in either $\bar{\eta}$ or w plane. In this last case, which take origins from classical implementation of Fredholm factorization [16], again we need to resort to difference equations for analytical continuation.

$$H_{oz+}(w) = \frac{2jH_o \pi \csc w \sin \frac{\pi w}{\gamma}}{-k\gamma \cos \frac{\pi w}{\gamma} + k\gamma \cos \frac{\pi \varphi_o}{\gamma}},\ H_{az+}(w) = -\frac{2jH_o \pi \csc w \sin \frac{\pi w}{\gamma}}{k\gamma \cos \frac{\pi w}{\gamma} + k\gamma \cos \frac{\pi \varphi_o}{\gamma}} \tag{89}$$

5.2. Regularized Integral Equation Method for the Direct Solution of the GWHEs in Angular Regions (Direct Fredholm Factorization)

Following the procedure of Section 3, that are simplified because of isotropic medium, we duplicate the equations. For E_z polarization we have

$$\begin{aligned} H_{o\rho}(\eta) &= H_{a\rho}(-m) \\ H_{a\rho}(\eta) &= H_{o\rho}(-m) \end{aligned} \tag{90}$$

while for H_z polarization we have

$$\begin{aligned} \xi H_{oz}(\eta) &= [\eta \sin(\gamma) + \xi \cos(\gamma)] H_{az}(-m) \\ \xi H_{az}(\eta) &= [\eta \sin(\gamma) + \xi \cos(\gamma)] H_{oz}(-m) \end{aligned} \tag{91}$$

with $m = m(\eta)$ defined in (61). Notice that, applying (70) to each of (90)-(91), the duplicated equations assumes same CWHE forms, with just a replacement of $\bar{\eta}$ with $-\bar{\eta}$.

Both systems of equations can be considered a particular case of

$$\begin{aligned} G(\eta)F_+(\eta) &= H(\eta)X_+(-m) \\ G_a(\eta)X_+(\eta) &= H_a(\eta)F_+(-m) \end{aligned} \tag{92}$$

that are suitable to describe more general cases. To describe the procedure, for simplicity, let us assume that $F_+(\eta)$ is a non-standard plus η unknown while $X_+(-m)$ is a standard minus m unknown; generalization is possible with a little effort.

Applying the Cauchy decomposition formula (49) to the unknowns defined in $-m(\eta)$

$$\begin{aligned} F_+(-m) &= \tfrac{1}{2\pi j}\int_{-\infty}^{\infty} \tfrac{F_+(\eta')}{\eta'+m}d\eta' + F_+^{n.s.}(-m),\ \eta \in \mathbb{R} \\ X_+(-m) &= \tfrac{1}{2\pi j}\int_{-\infty}^{\infty} \tfrac{X_+(\eta')}{\eta'+m}d\eta',\ \eta \in \mathbb{R} \end{aligned} \tag{93}$$

from (92) we obtain a system of integral equations

$$\begin{aligned} G(\eta)F_+(\eta) &= \tfrac{1}{2\pi j}H(\eta)\int_{-\infty}^{\infty} \tfrac{X_+(\eta')}{\eta'+m(\eta)}d\eta' \\ G_a(\eta)X_+(\eta) &= \tfrac{1}{2\pi j}H_a(\eta)\int_{-\infty}^{\infty} \tfrac{F_+(\eta')}{\eta'+m(\eta)}d\eta' + H_a(\eta)F_+^{n.s.}(-m(\eta)) \end{aligned} \tag{94}$$

that are not a system of Fredholm integral equations of second kind (non-compact kernel). To regularize (94) we follow the procedure presented in section 3. Performing a smile integration of (94), after mathematical manipulation, we have on the LHSs respectively

$$\begin{aligned} \tfrac{1}{2\pi j}\int_{\gamma_{1t}} \tfrac{G(t)F_+(t)}{t-\eta}dt &= G(\eta)F_+(\eta) + \tfrac{1}{2\pi j}\int_{-\infty}^{\infty} \tfrac{(G(t)-G(\eta))F_+(t)}{t-\eta}dt - G(\eta)F_+^{ns}(\eta) \\ \tfrac{1}{2\pi j}\int_{\gamma_{1t}} \tfrac{G_a(t)X_+(t)}{t-\eta}dt &= G_a(\eta)X_+(\eta) + \tfrac{1}{2\pi j}\int_{-\infty}^{\infty} \tfrac{(G_a(t)-G_a(\eta))X_+(t)}{t-\eta}dt \end{aligned} \tag{95}$$

and on the RHSs respectively

$$\frac{1}{2\pi j}\int_{\gamma_{1t}} \frac{1}{2\pi j}\frac{H(t)}{t-\eta}\int_{-\infty}^{\infty} \frac{X_+(\eta')}{\eta'+m(t)}d\eta'dt = \frac{1}{(2\pi j)^2}\int_{-\infty}^{\infty} M(\eta,\eta')X_+(\eta')d\eta' \tag{96}$$

and

$$\begin{aligned} \tfrac{1}{2\pi j}\int_{\gamma_{1t}} \tfrac{1}{2\pi j}\tfrac{H_a(t)}{t-\eta}\int_{-\infty}^{\infty} \tfrac{F_+(\eta')}{\eta'+m(t)}d\eta'dt &= \tfrac{1}{(2\pi j)^2}\int_{-\infty}^{\infty} M_a(\eta,\eta')F_+(\eta')d\eta' \\ \tfrac{1}{2\pi j}\int_{\gamma_{1t}} \tfrac{H_a(t)}{t-\eta}F_+^{ns}(-m(t))dt &= \tfrac{1}{2\pi j}\int_{-\infty}^{\infty} \tfrac{[H_a(t)-H_a(\eta)]F_+^{ns}(-m(t))}{t-\eta}dt + \tfrac{H_a(\eta)}{2\pi j}\int_{\gamma_{1t}} \tfrac{F_+^{ns}(-m(t))}{t-\eta}dt \end{aligned} \tag{97}$$

where

$$\begin{aligned} M(\eta,\eta') &= \int_{\gamma_{1t}} \tfrac{H(t)}{(t-\eta)(\eta'+m(t))}dt = \int_{-\infty}^{\infty} \tfrac{H(t)-H(\eta)}{(t-\eta)(\eta'+m(t))}dt + H(\eta)\int_{\gamma_{1t}} \tfrac{1}{(t-\eta)(\eta'+m(t))}dt \\ M_a(\eta,\eta') &= \int_{\gamma_{1t}} \tfrac{H_a(t)}{(t-\eta)(\eta'+m(t))}dt = \int_{-\infty}^{\infty} \tfrac{H_a(t)-H_a(\eta)}{(t-\eta)(\eta'+m(t))}dt + H_a(\eta)\int_{\gamma_{1\eta}} \tfrac{1}{(t-\eta)(\eta'+m(t))}dt \end{aligned} \tag{98}$$

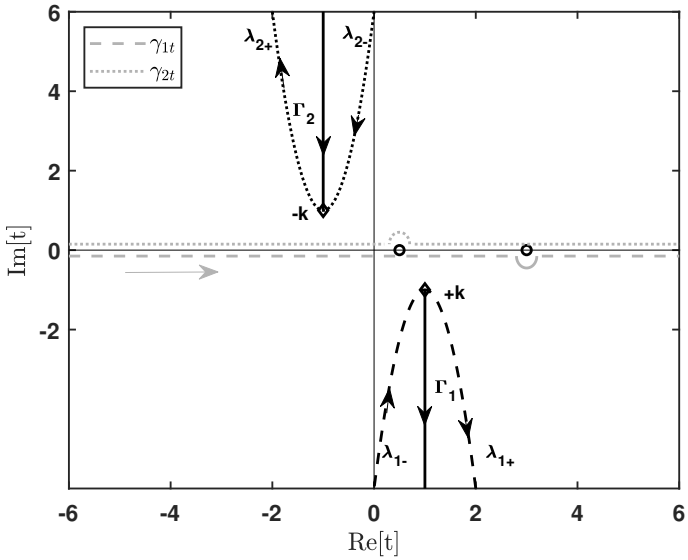

Figure 5. Vertical branch cuts $\Gamma_{1,2}$ of $m(t)$ originated in branch point $\pm k$ assuming lossy medium (for visibility $k = 1 - j$), and *smile* contour integration line γ_{1t} and *frown* contour integration line γ_{2t} with corresponding warped contours λ_1 and λ_2 wrapped around the vertical branch cuts Γ_1 and Γ_2. Note that γ_{1t} and γ_{2t} assume in the figure different observation points for indentation.

Merging (95) and (96)-(98) we get FIEs

$$G(\eta)F_+(\eta) + \frac{1}{2\pi j}\int\limits_{-\infty}^{\infty}\frac{(G(t)-G(\eta))F_+(t)}{t-\eta}dt = \frac{1}{(2\pi j)^2}\int\limits_{-\infty}^{\infty}M(\eta,\eta')X_+(\eta')d\eta' + G(\eta))F_+^{ns}(\eta) \tag{99}$$

$$\begin{aligned} &G_a(\eta)X_+(\eta) + \tfrac{1}{2\pi j}\int\limits_{-\infty}^{\infty}\tfrac{(G_a(t)-G_a(\eta))X_+(t)}{t-\eta}dt \\ &= \tfrac{1}{(2\pi j)^2}\int\limits_{-\infty}^{\infty}M_a(\eta,\eta')F_+(\eta')d\eta' + \tfrac{1}{2\pi j}\int\limits_{-\infty}^{\infty}\tfrac{(H_a(t)-H_a(\eta))F_+^{ns}(-m(t))}{t-\eta}dt + \tfrac{H_a(\eta)}{2\pi j}\int\limits_{\gamma_{1t}}\tfrac{F_+^{ns}(-m(t))}{t-\eta}dt \end{aligned} \tag{100}$$

We observe that from a computational point of view, the regularized FIEs (99) and (100) are particular efficient due to the presence of compact kernels integrated along the real axis except for the smile integration included in (98)

$$M_e(\eta,\eta') = \int\limits_{\gamma_{1t}}\frac{1}{(t-\eta)(\eta'+m(t))}dt \tag{101}$$

The evaluation of integral (101) can be effectively performed by warping the *smile* contour γ_{1t} in the lower half complex plane t into the integration path λ_1 wrapped around the vertical branch cut Γ_1 of $m(t)$ (61) originated in branch point $+k$, see Fig. 5. By collapsing the λ_1 onto Γ_1 we get

$$M_e(\eta,\eta') = \int_{\Gamma_1}\Delta(\frac{1}{(t-\eta)(\eta'+m(t)}\,)dt \tag{102}$$

where

$$\Delta(\frac{1}{(t-\eta)(\eta'+m(t)}\,) = -\frac{4\sqrt{(k-t)(k+t)}\sin(\gamma)}{(t-\eta)[-k^2+2(t^2+\eta'^2)-4t\eta'\cos(\gamma)+k^2\cos(2\gamma)]} \tag{103}$$

Assuming $t = k - jv$ $(v > 0)$ the representation (102) is quickly numerically convergent. A closed form expression of (102) is obtainable after considering:

1. selection of branch cut Γ_1 as the line $t = ku$ (with real $u > 1$) with consequent change of λ_1 and use of mapping $t = ku$ under integration sign,
2. expansion of (103) with minimal denominator,
3. careful mathematical manipulation of multivalued functions.

We get

$$M_e(\eta,\eta') = -2\sin(\gamma)\left(\frac{F_\infty(u_1(\eta))}{(u_1(\eta)-u_2(\eta'))(u_1(\eta)-u_3(\eta'))} - \frac{F_\infty(u_2(\eta'))}{(u_1(\eta)-u_2(\eta'))(u_2(\eta')-u_3(\eta'))} + \frac{F_\infty(u_3(\eta'))}{(u_1(\eta)-u_3(\eta'))(u_2(\eta')-u_3(\eta'))}\right) \tag{104}$$

with

$$F_\infty(u) = ju\log(2) - \sqrt{1-u^2}\log(-u + j\sqrt{1-u^2}) \tag{105}$$

and the poles

$$u_1(\eta) = \eta/k,\ u_2(\eta') = \frac{\eta'\cos\gamma - \sqrt{k^2-\eta'^2}\sin\gamma}{k},\ u_3(\eta') = \frac{\eta'\cos\gamma + \sqrt{k^2-\eta'^2}\sin\gamma}{k} \tag{106}$$

Let us now go back to particular cases and consider equations for H_z polarization (91) for a PEC angular region 1 written in the form (92) with the following definitions

$$F_+(\eta) = H_{oz}(\eta),\ X_+(\eta) = H_{az}(\eta),\ G(\eta) = G_a(\eta) = \frac{\xi}{\eta\sin(\gamma) + \xi\cos(\gamma)},\ H(\eta) = H_a(\eta) = 1 \tag{107}$$

The set of FIEs (99)-(100) simplifies: in particular $M(\eta,\eta') = M_a(\eta,\eta') = M_e(\eta,\eta')$ and reduces to (102). Eq. (99)-(100) respectively becomes the system of FIEs

$$G(\eta)H_{oz}(\eta) + \frac{1}{2\pi j}\int_{-\infty}^{\infty}\frac{(G(t)-G(\eta))H_{oz}(t)}{t-\eta}dt = \frac{1}{(2\pi j)^2}\int_{-\infty}^{\infty}M_e(\eta,\eta')H_{az}(\eta')d\eta' + s_1(\eta) \tag{108}$$

and

$$G(\eta)H_{az}(\eta) + \frac{1}{2\pi j}\int_{-\infty}^{\infty}\frac{(G(t)-G(\eta))H_{az}(t)}{t-\eta}dt = \frac{1}{(2\pi j)^2}\int_{-\infty}^{\infty}M_e(\eta,\eta')H_{oz}(\eta')d\eta' + s_2(\eta) \tag{109}$$

with

$$s_1(\eta) = G(\eta)H_{oz}^{ns}(\eta),\quad s_2(\eta) = \frac{1}{2\pi j}\int_{\gamma_{1t}}\frac{H_{oz}^{ns}(-m(t))}{t-\eta}dt \tag{110}$$

Let us focus the attention on the source term (110) and, for simplicity, assume that only $F_+(\eta) = H_{oz}(\eta)$ is non-standard:

$$F_+^{ns}(\eta) = H_{oz}^{ns}(\eta) = \frac{2jH_o}{\eta-\eta_o} \tag{111}$$

with $\eta_o = -k\cos(\varphi_o)$, $0 < \varphi_o < \pi/2$ and k with small losses ($k = k_r - jk_i$, $k_i << k_r$). From (111), according to $-m(\eta)$ properties, see also Fig. 4, $H_{oz}^{ns}(-m(\eta))$ shows in the proper lower half complex plane η poles originated by the zeros of $m(\eta) + \eta_o$ (in m plane we have the pole $m_o = -\eta_o$). The poles can be related to GO waves, i.e. connected to the last couple of reflections from faces a and o that create shadow boundaries, for instance see [14]. For example if $\varphi_o < \pi - \gamma$, we have one reflection from face a and one reflection from face o reflected again by face a. In fact, from a mathematical point of view, in this case we have that the pole m_o is related to the poles $\eta_{ra} = -k\cos(\gamma - \varphi_o)$ (reflection from face a) and $\eta_{raro} = -k\cos(\gamma + \varphi_o)$ (reflection from a after o) associated to incoming azimuthal directions $\gamma \mp \varphi_o$ with respect to reference face a, i.e. incoming directions $2\gamma \mp \varphi_o$ with respect to face o. However, we also need to note that residues of poles in the selected test problems are related always only to incident field. It means that the primary spectra of $H_{oz}^{ns}(-m(\eta))$ in (110) is more similar to a replica of incident spectrum for η_{ra}, η_{raro}, similarly to what has been described in [17] in w plane.

Indeed, the integrand of source term (110) also exhibits the branch cut of $-m(\eta)$ thus we estimate (110) by warping γ_{1t} into λ_1

$$s_2(\eta) = \frac{1}{2\pi j}\int\limits_{\lambda_1} \frac{H_{oz}^{ns}(-m(t))}{t-\eta}dt + \frac{R_a}{\eta-\eta_{ra}} + \frac{R_{ao}}{\eta-\eta_{raro}} \tag{112}$$

where R_a and R_o are respectively the residues of $H_{oz}(-m(\eta))$ in η_{ra} and η_{raro}:

$$H_{oz}^{ns}(-m(\eta)) = -\frac{2jH_o}{m(-\eta)+\eta_o} = \frac{T_{m_o}}{m(-\eta)+\eta_o},\ T_{m_o} = -2jH_o \tag{113}$$

$$R_{a,ao} = T_{m_o}\frac{d\eta}{dm}\bigg|_{\eta_{ra},\eta_{raro}} = \frac{2jH_o}{\cos\gamma + \frac{\eta\sin\gamma}{\sqrt{k^2-\eta^2}}}\bigg|_{\eta_{ra},\eta_{raro}} \tag{114}$$

Using the same passage that in (102) for (101) to (112), we get

$$\frac{1}{2\pi j}\int\limits_{\lambda_1} \frac{H_{oz}^{ns}(-m(t))}{t-\eta}dt = \frac{H_o}{\pi}\int_{\lambda_1}\frac{1}{(t-\eta)(-m(t)-\eta_o)}dt = -\frac{H_o}{\pi}M_e(\eta,\eta_o) \tag{115}$$

thus

$$s_2(\eta) = -\frac{H_o}{\pi}M_e(\eta,\eta_o) + \frac{R_a}{\eta-\eta_{ra}} + \frac{R_{ao}}{\eta-\eta_{raro}} \tag{116}$$

The final set of FIEs for H_z polarization when illuminated by a plane wave with $0 < \varphi_o < \pi/2$ are then (108)-(109) (a specialization of (99)-(100)) with sources $s_{1,2}(\eta)$ defined and calculated in (110), (111), (116). Note that $s_1(\eta)$ and $s_2(\eta)$ are respectively a spectral component defined in η plane of $H_{oz}(\eta)$ and $H_{az}(\eta)$, i.e. with the reference coordinate system of face o and face a.

Let us now examine the convergence properties of FIEs (108)-(109) to get accurate numerical results [47]. According to classical Fredholm factorization method [19], the regularization procedure provides compact kernels of the type reported in LHS of (108)-(109), i.e. square integrable. The further integral operator reported on the RHS of (108)-(109) in terms of $M_e(\eta,\eta')$ is related to coupling term between the spectra of delimiting faces. This kernel is again compact because (101) shows that $M_e(\eta,\eta')$ is never singular as $\eta \neq t$ and $\eta' \neq m(t)$ and, (104) shows that $M_e(\eta,\eta')$ is square integrable according to its asymptotic behavior in terms of (106). Similar considerations can be repeated to more complex and general cases of angular region immersed in/made of arbitrary linear media.

5.3. Implementation of Numerical Example and Validation of Direct Fredholm Factorization

Let us consider region 1 of Fig. 1 of aperture angle $\pi/2 < \gamma < \pi$, filled by a homogeneous isotropic medium with propagation constant k ($k = k_r - jk_i$, $k_i << k_r$) and terminated by PEC boundary condition. The angular region is illuminated by a H_z polarized plane wave with incoming direction φ_o ($0 < \varphi_o < \pi - \gamma$) and intensity H_o. The spectral solution $(H_{oz}(\eta), H_{az}(\eta))$ can be provided by the system of FIEs (108)-(109). Due to the convergence properties of the kernel [47], simple sample and hold approximation is enforced with truncation of integration intervals at $\pm A$ and integration step h, such that $A/h \in \mathbb{N}$. We tested our novel direct FIE solution against the classical exact closed form solution provided in subsection 5.1 in η and w planes respectively (88) and (89). Furthermore we compared asymptotic results in terms of GTD coefficients. We examine in detail the case where $\gamma = 0.7\pi$, $k = 1 - j0.1$, $H_o = 1A/m$, $\varphi_o = 0.1\pi$. Since we have $0 < \varphi_o < \pi - \gamma$, GO field is constituted by incident, face a reflected and double reflected (from face o and then from face a) waves and only the plus spectral unknown along face o, i.e. $H_{oz}(\eta)$, is non standard in the WH formulation (91), as reported in the example of previous subsection. To enhance the convergence of the approximate FIE solution given

by (108)-(109), we warp the integration line constituted by the real axis into a straight line located in the 1st and 3rd quadrant of the complex plane at an angle θ with respect to the real axis (the singularities of the kernel and the sources are located in the 2nd and 4th quadrant, see §5.3, §5.4 of [16]):

$$\alpha_t(t) = t\exp^{j\theta},\ t \in \mathbb{R},\ 0 < \theta < \pi/2 \tag{117}$$

According to the physical parameters of the test problem we have $\eta_{ra} = 0.309017 - 0.0309017j$, $\eta_{raro} = 0.809017 - 0.0809017j$, both located in the lower half plane, thus considered in (116). The discretization of (108)-(109) by sample and hold with A, h yields a linear system of equation of dimensions $2(2(A/h)+1)$

$$\left|\begin{array}{cc} \underline{\underline{d}}_G + \underline{\underline{K}}_G & -\underline{\underline{M}}_e \\ -\underline{\underline{M}}_e & \underline{\underline{d}}_G + \underline{\underline{K}}_G \end{array}\right| \left|\begin{array}{c} \underline{H}_{oz} \\ \underline{H}_{az} \end{array}\right| = \left|\begin{array}{c} \underline{s}_1 \\ \underline{s}_2 \end{array}\right| \tag{118}$$

where the diagonal matrix $\underline{\underline{d}}_G$, the matrix $\underline{\underline{K}}_G$ and the matrix $\underline{\underline{M}}_e$ contain respectively sample of $G(\eta)$, $\frac{G(t)-G(\eta)}{t-\eta}$ and $M_e(\eta,\eta')$, while the vectors $\underline{H}_{oz}$, $\underline{H}_{az}$, $\underline{s}_1$, $\underline{s}_2$ contain samples respectability $H_{oz}(\eta)$, $H_{az}(\eta)$, $s_1(\eta)$, $s_2(\eta)$. Note that $\underline{\underline{M}}_e$ is the coupling matrix that is much weaker than the remaining terms. The sampled solution allow to build a representation of $H_{oz}(\eta)$, $H_{az}(\eta)$ substituting them into the integral part of (108)-(109):

$$H_{oz,az}(\eta) = -\frac{h}{2\pi j}\sum_{-A/h}^{A/h}\frac{[G^{-1}(\eta)G(\alpha_t(hi))-1]H_{oz,az}(\alpha_t(hi))}{\alpha_t(hi)-\eta} + \frac{hG^{-1}(\eta)}{(2\pi j)^2}\sum_{-A/h}^{A/h} M_e(\eta,\alpha_t(hi))H_{az,oz}(\alpha_t(hi)) + G^{-1}(\eta)s_{1,2}(\eta) \tag{119}$$

These approximate expressions of $H_{oz}(\eta)$, $H_{az}(\eta)$ are valid for analytic continuation in the proper sheet of η plane useful to correctly estimate fields in physical domain through asymptotics of half-planes as discussed in Section 4. This property limits the requirement to know the spectra only in the proper sheet as acquired in the procedure, that is a novelty and a progress with respect to classical Fredholm factorization combined with spectral mapping in GWHE wedge problems.

To highlight the performance of the method, we compare the spectra along the real axis of η plane and the segment of η plane useful for asymptotics according to Steepest Descent Path (SDP) method that in isotropic medium corresponds to $\eta = -k\cos w$ with $-\pi < w < 0$, i.e the segment that connect $-k$ with k.

To study convergence of the method we have selected physical parameters of region 1 with an aperture angle $\gamma = 0.7\pi$ and plane wave illumination at H_z polarization with $H_o = 1A/m$, $\varphi_o = 0.1\pi$, $k = 1 - j0.1$. We selected quadrature parameters $5 \leq A \leq 40$, $0.2 \leq h \leq 0.25$, $\theta = 0.1$ such that $A/h \in \mathbb{N}$. Numerical results are provided in Fig. 6 along the segment for asymptotic estimation. From the figure we notice that along the segment we have a degradation of spectral solution near $w = -\pi, 0$ which correspond to $\eta = k, -k$. We recall that the solution of FIEs have been obtained by simple sample and hold quadrature and estimation of $M_e(\eta,\eta')$ that saturate precision in particular near $\eta = k, -k$ (the branch point $\eta = -k$ is a local offending singularity for the plus spectra that should not appear while $\eta = k$ is related to physical structural properties of the problem). Improvement would be obtained with specialized quadrature (and method of moments) capable of taking into account non algebraic behavior such as branch points [48,49]. However, the scope of the present method is to get very simple, fast and convergent solution that cannot incorporate sophisticated quadratures. Furthermore, we observe that the lack on precision near $\eta = k, -k$ is mitigated while computing asymptotics since plus spectral unknowns are multiplied by $\sin w$ providing locally smoothing errors. However, while the offending $\eta = -k$ is a very local perturbation, the physical $\eta = k$ is more present as it is physical.

To recover the quality of solution near $w = -\pi, 0$ ($\eta = k, -k$) we resort to spectral considerations based on the properties of the original GWHEs formulation (91). Eqs. (91) can be applied to the approximate solutions obtained from the FIEs to get a new

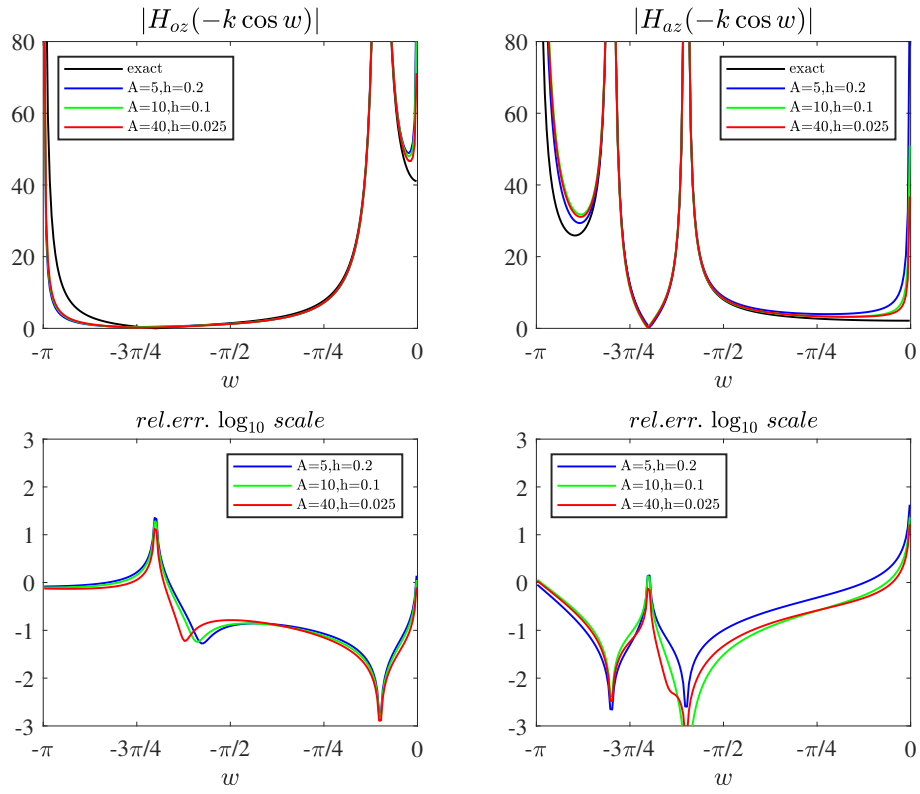

Figure 6. On top, plots of absolute value of the spectral solutions $|H_{oz}(-k\cos w)|$ and $|H_{az}(-k\cos w)|$ obtained as exact solution and with the FIE approximation for different A, h. On bottom corresponding relative errors between the exact solution and the FIE solutions for different A, h in $\log_{10}$ scale. We observe a degradation of spectral solution near $w = -\pi, 0$ which correspond to $\eta = k, -k$. The branch point $\eta = -k$ is an offending singularity for the plus spectra while $\eta = k$ is related to physical structural properties of the problem.

representations of plus spectra from the FIE approximated spectra. This application allows to obtain spectra near $w = -\pi, 0$ ($\eta = k, -k$) that takes origin from other portion of η plane according to $m(\eta)$. This procedure is particularly effective and valid because $m(\eta)$ with η in the proper sheet is a portion of the proper sheet of η plane. To demonstrate this property is particular effective to rewrite (in this simplified isotropic problem) (91) in w plane:

$$\begin{aligned} H_{oz}(-k\cos w) &= \frac{-n(-k\cos w)}{\xi(-k\cos w)} H_{az}(-k\cos(w+\gamma)) \\ H_{az}(-k\cos w) &= \frac{-n(-k\cos w)}{\xi(-k\cos w)} H_{oz}(-k\cos(w+\gamma)) \end{aligned} \tag{120}$$

with $\xi(-k\cos w) = -k\sin w$, $-n = -k\sin(w+\gamma)$. We notice that $-\pi < w < 0$ on the LHS corresponds to $-\pi+\gamma < w < \gamma$ on the RHS due to $(m = k\cos(w+\gamma))$, where the unknowns are correctly computed. This methodology (named iteration) re-imposes GWHEs on the initial FIE approximate spectra and it shifts the lack of precision to a region where the spectral solution is good yielding an homogenization of the error level, see Fig. 7. In the figure we have reported the exact solution and approximate solutions obtained from the quadrature of FIE with $A = 40, h = 0.025$, from the quadrature of FIE with $A = 40, h = 0.025$ plus the application of (91), and from the application of (91) to the sources sources of FIE ignoring integrals terms, i.e. using $H_{oz,az}(\eta) = +G^{-1}(\eta)s_{1,2}(\eta)$.

Note that, considering (91), the map in (120) is only limited, thus we cannot interpret this procedure as a first iteration on the application of contraction theorem. In fact from our studies, successive iterations do not yield any benefit in the convergence of the solution. This is also justified by the fact in w plane the multiple applications of (120) correspond to recursive equations/difference equations that further shift spectra in w plane, navigating

replica of proper and improper sheet, see [17], [15]. Moreover, we exclude also that the map can compensate all physical behavior of the problem starting from roughly approximate solutions. In Fig. 7 we show the importance of the quality of starting spectra originated from the solution of FIE before the application of (120). We finally observe that while the

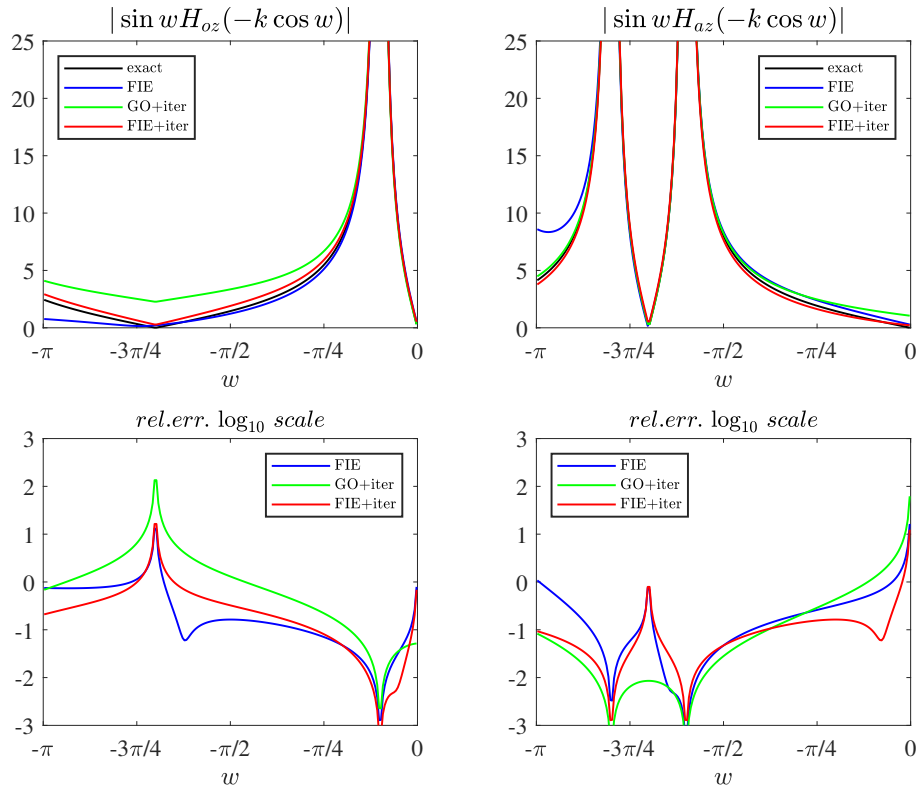

Figure 7. On top, plots of absolute value of the spectral solutions $|\sin w\, H_{oz}(-k\cos w)|$ and $|\sin w\, H_{az}(-k\cos w)|$ obtained as exact solution and with 1) the FIE with $A = 40, h = 0.025$, 2) the FIE plus the application of on iteration of (91) (FIE+iter), 3) the application of (91) to the source terms of the FIE (GO+iter). On bottom corresponding relative errors between the exact solution and the approximated solutions. We observe an improvement of solution near $w = -\pi, 0$ once we apply an iteration of (91) to the approximate solution from FIE yielding an homogenization of error.

FIE provide good spectra except near the branch cuts, the iteration (91) enforce the correct modeling of structural spectral properties such as the branch cuts.

To further compare the solutions and validate the proposed procedure we compute the GTD diffraction coefficients as outlined in Section 4 by asymptoptics. Using superposition we can compute the diffraction by applying asymptotics individually to the spectral solutions at faces o and a considering only homogeneous terms in (56), (59) taking care of the different reference coordinates (see discussion at Sections 3- 4 while considering region 1 characterized by γ as a region 2' characterized by $\pi - \gamma$, see Fig. 2, (45), (59)):

$$\tilde{\boldsymbol{\psi}}_{\boldsymbol{y}}^{\boldsymbol{ho}}(\eta, v) = \sum_{i=1}^{2} \boldsymbol{v_i} \cdot \tilde{\boldsymbol{\psi}}_{\boldsymbol{y}}(\eta, 0) e^{-\lambda_{\gamma i}(\gamma)\, v} \boldsymbol{u_i},\ v > 0 \tag{121}$$

$$\tilde{\boldsymbol{\psi}}_{\boldsymbol{Y1}}^{\boldsymbol{ho}}(\eta, v) = \sum_{i=3}^{4} \boldsymbol{v_{iY_1}} \cdot \tilde{\boldsymbol{\psi}}_{\boldsymbol{Y1}}(\eta, 0) e^{-\lambda_{\gamma i Y_1}(\pi-\gamma)\, v} \boldsymbol{u_{iY_1}},\ v < 0 \tag{122}$$

Let us start from the inversion of face o contribution (121):

$$\boldsymbol{\psi}_{\boldsymbol{y}}^{\boldsymbol{ho}}(u, v) = \frac{1}{2\pi} \int_{B_r} \tilde{\boldsymbol{\psi}}_{\boldsymbol{y}}^{\boldsymbol{ho}}(\eta, v) e^{-j\eta u} d\eta \tag{123}$$

According to coordinate mapping (18), from (16) and (23), we have

$$-\lambda_{\gamma i}(\gamma)\, v - j\eta u = -j\eta\cos\gamma\, v - j\xi_i \sin\gamma v - j\eta(x - v\cos\gamma) = -j(\eta x + \xi_i y),\ i = 1,2 \quad (124)$$

with $\xi_i = \xi$, $i = 1,2$ thus

$$\boldsymbol{\psi}_{\boldsymbol{y}}^{\boldsymbol{ho}}(x,y) = \frac{1}{2\pi}\int_{B_r}\sum_{i=1}^{2} \boldsymbol{v_i}\cdot\tilde{\boldsymbol{\psi}}_{\boldsymbol{y}}(\eta,0)\boldsymbol{u_i} e^{-j(\eta x+\xi y)} d\eta \quad (125)$$

with B_r the Bromwich contour (over all singularities) whose asymptotic estimation at far field is composed of GO terms (captured poles) and GTD diffracted component (due to saddle point with the application of SDP method) in global cylindrical coordinate:

$$\boldsymbol{\psi}_{\boldsymbol{y}}^{\boldsymbol{ho,gtd}}(\rho,\varphi) = \sqrt{\frac{k}{2\pi\rho}} e^{-j(k\rho-\pi/4)} \sum_{i=1}^{2} \boldsymbol{v_i}\cdot\tilde{\boldsymbol{\psi}}_{\boldsymbol{y}}(k\cos\varphi,0)\boldsymbol{u_i}\sin|\varphi| \quad (126)$$

that for our test problem (region 1 with PEC faces at H_z polarization) reduces to the third component

$$\boldsymbol{\psi}_{\boldsymbol{y}}^{\boldsymbol{ho,gtd}}(\rho,\varphi)[3] = H_{oz}^{gtd}(\rho,\varphi) = \sqrt{\frac{k}{2\pi\rho}} e^{-j(k\rho-\pi/4)} \frac{H_{oz}(k\cos\varphi)}{2}\sin|\varphi| \quad (127)$$

according to definition of $\tilde{\boldsymbol{\psi}}_{\boldsymbol{y}}(\eta,v)$ (3) and $\boldsymbol{u_i},\boldsymbol{v_i}$ reported at (62)-(63). We get the GTD diffraction coefficient component due to face o

$$D_{Hoz}^{gtd}(\varphi) = \frac{kH_{oz}(k\cos\varphi)\sin|\varphi|}{j2H_o} \quad (128)$$

Now we repeat the procedure starting from the inversion of face a contribution (122) using notation of Fig. 2.(b):

$$\boldsymbol{\psi}_{\boldsymbol{Y1}}^{\boldsymbol{ho}}(u,v) = \frac{1}{2\pi}\int_{B_r} \tilde{\boldsymbol{\psi}}_{\boldsymbol{Y1}}^{\boldsymbol{ho}}(\eta,v) e^{-j\eta u} d\eta \quad (129)$$

According to coordinate mapping

$$X_1 = u + v\cos(\pi-\gamma),\ Y_1 = v\sin(\pi-\gamma) \quad (130)$$

we have from (16) and (23)

$$-\lambda_{\gamma i Y_1}(\pi-\gamma)\, v - j\eta u = +j\eta\cos\gamma\, v + j\xi_i\sin\gamma v - j\eta(X_1 + v\cos\gamma) = -j\eta X_1 + j\xi_i Y_1,\ i = 3,4 \quad (131)$$

with $\xi_i = \xi$, $i = 3,4$ thus

$$\boldsymbol{\psi}_{\boldsymbol{Y1}}^{\boldsymbol{ho}}(X_1,Y_1) = \frac{1}{2\pi}\int_{B_r}\sum_{i=3}^{4} \boldsymbol{v_{iY_1}}\cdot\tilde{\boldsymbol{\psi}}_{\boldsymbol{Y1}}(\eta,0)\boldsymbol{u_{iY_1}} e^{-j\eta X_1 + j\xi Y_1} d\eta \quad (132)$$

with B_r the Bromwich contour whose asymptotic estimation at far field is composed of GO terms and GTD diffracted component in global cylindrical coordinate:

$$\boldsymbol{\psi}_{\boldsymbol{Y1}}^{\boldsymbol{ho,gtd}}(\rho,\varphi) = \sqrt{\frac{k}{2\pi\rho}} e^{-j(k\rho-\pi/4)} \sum_{i=3}^{4} \boldsymbol{v_{iY_1}}\cdot\tilde{\boldsymbol{\psi}}_{\boldsymbol{Y1}}(k\cos(\varphi-\gamma),0)\boldsymbol{u_{iY_1}}\sin|\varphi-\gamma| \quad (133)$$

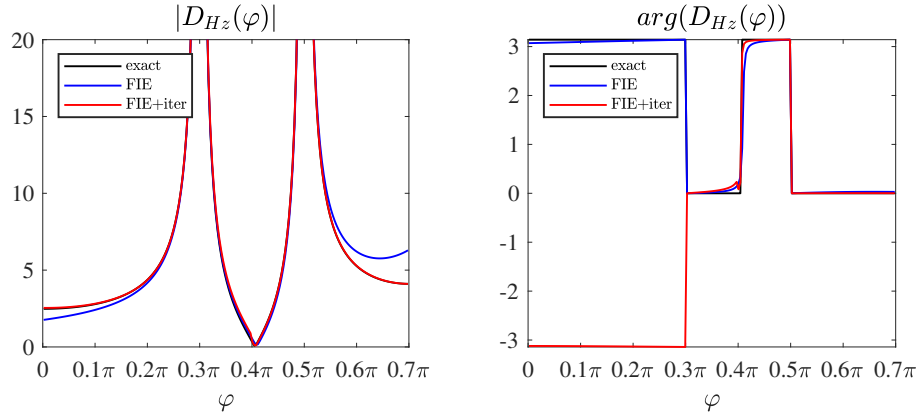

Figure 8. GTD diffraction coefficient (absolute value and phase) for the test problem under consideration: $\gamma = 0.7\pi$ and plane wave illumination at H_z polarization with $H_o = 1A/m$, $\varphi_o = 0.1\pi$, $k = 1 - j0.1$. In the figure we have reported the exact GTD together with the ones obtained following the FIE approximate estimation of the spectra without and with the application of an iteration, and selecting $A = 20, h = 0.05, \theta = 0.1$.

that for our test problem (region 1 with PEC faces at H_z polarization) reduces to the third component

$$\boldsymbol{\psi}_{\boldsymbol{Y1}}^{\boldsymbol{ho,gtd}}(\rho,\varphi)[3] = H_{az}^{gtd}(\rho,\varphi) = \sqrt{\frac{k}{2\pi\rho}}e^{-j(k\rho-\pi/4)}\frac{H_{az}(k\cos(\varphi-\gamma))}{2}\sin|\varphi-\gamma| \quad (134)$$

according to definition of $\tilde{\boldsymbol{\psi}}_{\boldsymbol{y}}(\eta,v)$ (3) and $\boldsymbol{u}_{\boldsymbol{iY_1}} = \boldsymbol{u}_{\boldsymbol{i}}, \boldsymbol{v}_{\boldsymbol{iY_1}} = \boldsymbol{v}_{\boldsymbol{i}}$ reported at (62)-(63). Note the invariance of $\boldsymbol{u}_{\boldsymbol{iY_1}} = \boldsymbol{u}_{\boldsymbol{i}}, \boldsymbol{v}_{\boldsymbol{iY_1}} = \boldsymbol{v}_{\boldsymbol{i}}$ in the rotation of reference system that is allowable only in isotropic regions otherwise for arbitrary linear media more complex procedure is required for their definitions, see Section 2.

Finally, we get the GTD diffraction coefficient component due to face a

$$D_{Haz}^{gtd}(\varphi) = \frac{kH_{az}(k\cos(\varphi-\gamma))\sin|\varphi-\gamma|}{j2H_o} \quad (135)$$

The complete GTD coefficient is just the sum for superposition of (128) and (135):

$$D_{Hz}^{gtd}(\varphi) = D_{Hoz}^{gtd}(\varphi) + D_{Haz}^{gtd}(\varphi) \quad (136)$$

Fig. 8 shows GTD diffraction coefficient for the test problem under consideration: $\gamma = 0.7\pi$ and plane wave illumination at H_z polarization with $H_o = 1A/m$, $\varphi_o = 0.1\pi$, $k = 1 - j0.1$. In the figure we have reported the exact GTD coefficient in term of absolute value and phase together with the ones obtained following the FIE approximate estimation of the spectra without and with the application of an iteration, and selecting $A = 20, h = 0.05, \theta = 0.1$. Fig. 9 shows the corresponding relative error on the GTD diffraction coefficient in $\log_{10}$ scale. We note, as expected, that the solution with the iteration is correct while the one without the iteration lacks in estimation near the faces of the angular regions, i.e. face o for $\varphi = 0$ and face a for $\varphi = \gamma$ because related respectively to the spectra of $H_{oz}(\eta)$ near $\eta = k$ (128) and of $H_{az}(\eta)$ near $\eta = k$ (135) ($\eta = k$ correspond to $w = -\pi$ and it is a physical branch cut). Note also that the spectra of $H_{oz}(\eta), H_{az}(\eta)$ near $\eta = -k$ ($w = 0$) is not used for GTD computation, thus the lack of possible precision in the offending branch point does not impact on the solution. Moreover, the change of slope and level of the relative error in Fig. 9 is obtained by the reported algorithm to improve the quality of the approximate solution given by the direct application of Fredholm factorization. In fact FIE+iteration implements the computation of GTD diffraction coefficient (136) via (128) and (135) where the spectra $H_{oz}(-k\cos w)$ and $H_{az}(-k\cos w)$ are obtained by enforcing (120)

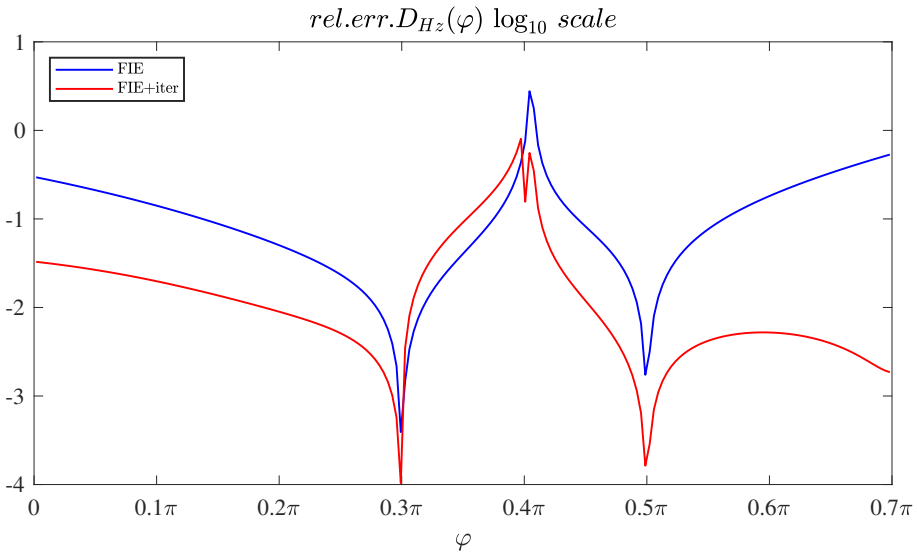

Figure 9. Relative error on GTD diffraction coefficient in $\log_{10}$ scale corresponding to results of Fig. 8.

on the approximate spectra obtained by the direct application of Fredholm factorization. This procedure mixes spectral resolution properties of the two faces, improving the quality of the spectra in particular recovering the degradation of spectral resolution near $w = \pi, 0$, i.e. $\eta = k, -k$.

Finally, we comment that the direct implementation of FIE in w plane yields high precision results in isotropic angular region problem [16] that exceeds the precision of the current procedure in terms of spectra; however we recall that the scope of the present work is to present an effective procedure to compute diffraction implementable in problems where w plane cannot be defined as in arbitrarily linear media.

6. An Example of Application of the Functional Equations in Complex Media: Scattering from a PEC Half-Plane in Gyrotropic Medium

The scattering of a plane electromagnetic wave at normal incidence by a perfectly conducting semi-infinite screen embedded in a homogeneous gyrotropic medium (such as plasma) is presented in this section with the scope to validate the proposed method, the functional equations and WH equations in non isotropic media. Since our formulation is in terms of field components we have selected as comparative studies [21,22,26,27] with respect to other works that employ definitions in terms of potentials. We have selected in particular the work [21] where the distinguished axis of the electric gyrotropic medium is parallel to the edge of the halfplane, i.e. as in plasma with uniform magnetic field impressed along the edge direction. This medium enforces in our reference system of coordinates (z, x, y) a tensorial electric permittivity

$$\underline{\underline{\varepsilon}} = \begin{bmatrix} \varepsilon_3 & 0 & 0 \\ 0 & \varepsilon_1 & +j\varepsilon_2 \\ 0 & -j\varepsilon_2 & \varepsilon_1 \end{bmatrix} \tag{137}$$

with z as distinguished axis and $\underline{\underline{\mu}} = \mu_o \underline{\underline{I}}$, $\underline{\underline{\xi}} = \underline{\underline{\zeta}} = \underline{\underline{0}}$. As reported in [21] this vector problem is separable into two equivalent scalar problems for E_z (H-mode) and H_z (E-mode) polarizations.

By applying the procedure described in previous Section 2 and with simplified definitions of the quantities reported in Appendix A we obtain (progressive, regressive) eigenvalues

$$\lambda_{1,3} = \pm\sqrt{\eta^2 - k_1^2} = \pm j\xi_1, \quad \lambda_{2,4} = \pm\sqrt{\eta^2 - k_2^2} = \pm j\xi_2 \tag{138}$$

with $k_1^2 = \omega^2\mu_o\varepsilon/\varepsilon_1 = k_o^2\varepsilon/\varepsilon_1$, $k_2^2 = \omega^2\mu_o\varepsilon_3 = k_o^2\varepsilon_{r3}$, $\varepsilon_{ri} = \varepsilon_i/\varepsilon_o$, $\varepsilon = \varepsilon_1^2 - \varepsilon_2^2$, $k_o = \omega\sqrt{\varepsilon_o\mu_o}$.

The corresponding eigenvectors $\boldsymbol{u_i}$, from which we easily compute also the reciprocal vectors $\boldsymbol{v_i}$ by inversion, are

$$\boldsymbol{u_1} = \begin{vmatrix} 0 \\ \frac{j(-\varepsilon_2\eta+\varepsilon_1 j\xi_1)}{\varepsilon\omega} \\ 1 \\ 0 \end{vmatrix}, \boldsymbol{u_2} = \begin{vmatrix} \frac{\mu_o\omega}{\varepsilon_2} \\ 0 \\ 0 \\ 1 \end{vmatrix}, \boldsymbol{u_3} = \begin{vmatrix} 0 \\ -\frac{j(\varepsilon_2\eta+\varepsilon_1 j\xi_1)}{\varepsilon\omega} \\ 1 \\ 0 \end{vmatrix}, \boldsymbol{u_4} = \begin{vmatrix} -\frac{\mu_o\omega}{\varepsilon_2} \\ 0 \\ 0 \\ 1 \end{vmatrix} \tag{139}$$

The problem shows simplification because of $\gamma = \pi$, see for instance the impact of the anisotropies on (35) or

$$m = m_i(\pi - \gamma) = m_{i+2}(\gamma) = \eta; \quad i = 1,2 \tag{140}$$

However, we keep the procedure as general as possible, extendable to wedge problems, obtaining from (27) and (31)

$$\tilde{\boldsymbol{\psi}}_{\boldsymbol{sa}+}(-m_i(\gamma)) = \left| \; E_{az}\cos(\gamma), E_{a\rho} + \frac{\eta H_{az}\sin(\gamma)}{\omega\varepsilon_1}, H_{az}\cos(\gamma) - \frac{jH_{az}\varepsilon_2\sin(\gamma)}{\varepsilon_1}, H_{a\rho} - \frac{E_{az}\eta\sin(\gamma)}{\mu_o\omega} \; \right|^t \tag{141}$$

From here on we omit the spectral dependence in field components for compactness of formulae. Applying (32) we get in explicit form the following two functional equations for region 1:

$$E_{ox}\omega\varepsilon + H_{oz}\xi_1\varepsilon_1 + j\eta H_{oz}\varepsilon_2 = H_{az}[\sin(\gamma)(\eta\varepsilon_1 - j\xi_1\varepsilon_2) + \cos(\gamma)(\xi_1\varepsilon_1 + j\eta\varepsilon_2)] + E_{a\rho}\varepsilon\omega \tag{142}$$

$$H_{ox}\mu_o\omega - E_{oz}\xi_2 = H_{a\rho}\mu_o\omega \tag{143}$$

Similarly the procedure can be repeated for region 2. The complete set of equations highlights the decoupling of E_z from H_z polarization. Applying the PEC boundary conditions on the faces we get respectively for E_z na H_z polarizations after some manipulations:

$$\begin{cases} H_{ox} = \frac{H_{a\rho}}{2} + \frac{H_{b\rho}}{2} \\ -\frac{E_{oz}\xi_2}{\mu_o\omega} = \frac{H_{a\rho}}{2} - \frac{H_{b\rho}}{2} \end{cases} \tag{144}$$

$$\begin{cases} E_{ox}\omega\varepsilon + H_{oz}\xi_1\varepsilon_1 + j\eta H_{oz}\varepsilon_2 = H_{az}[\sin(\gamma)(\eta\varepsilon_1 - j\xi_1\varepsilon_2) + \cos(\gamma)(\xi_1\varepsilon_1 + j\eta\varepsilon_2)] \\ -E_{ox}\omega\varepsilon + H_{oz}\xi_1\varepsilon_1 - j\eta H_{oz}\varepsilon_2 = H_{bz}[\sin(\gamma)(\eta\varepsilon_1 + j\xi_1\varepsilon_2) + \cos(\gamma)(\xi_1\varepsilon_1 - j\eta\varepsilon_2)] \end{cases} \tag{145}$$

Now we impose $\gamma = \pi$, i.e. the angular regions are defined for the half-plane problem. From (144) we notice that E_z polarization behaves as half-plane problems immersed in classical isotropic regions [40] but with propagation constant $k_2^2 = \omega^2\mu_o\varepsilon_3 = k_o^2\varepsilon_{r3}$, i.e. network represetation with characteristic impedance $Z_{Ez} = \omega\mu_o/\xi_2$, confirming [21].

With further mathematical manipulating of (145) we get

$$\begin{cases} -2H_{oz} + \frac{2iE_{ox}\eta\omega\varepsilon\varepsilon_2}{\xi_1^2\varepsilon_1^2+\eta^2\varepsilon_2^2} = H_{az} + H_{bz} \\ -\frac{2E_{ox}\xi_1\omega\varepsilon\varepsilon_1}{\xi_1^2\varepsilon_1^2+\eta^2\varepsilon_2^2} = H_{az} - H_{bz} \end{cases} \tag{146}$$

The second equation of (146) shows the same WH kernel of eq. (25) in [21]

$$G_{H_z}^{-1} = -\frac{\xi_1^2\varepsilon_1^2 + \eta^2\varepsilon_2^2}{2\xi_1\omega\varepsilon\varepsilon_1} = -\frac{(k_1^2 - \eta^2)\varepsilon_1^2 + \eta^2\varepsilon_2^2}{2\sqrt{k_1^2 - \eta^2}\omega\varepsilon\varepsilon_1} = -\frac{k_1^2\varepsilon_1^2/\varepsilon - \eta^2}{2\sqrt{k_1^2 - \eta^2}\omega\varepsilon_1} \tag{147}$$

except for multiplication by a scalar. Moreover it is easily recognizable from the numerator the characteristic pole of surface wave phenomenon identified also in [21]. Solutions of the problem can be achieved with approximate techniques validated in previous sections or via classical procedure as in [21] but this item goes beyond the scope of this paper.

7. Conclusions

Spectral methods (such as SM,KL,WH) are well consolidated fundamental and effective tools for the correct and precise analysis of electromagnetic diffraction problems with one propagation constant, although not immediately applicable to multiple propagation constant problems.

In this paper we propose a comprehensive theoretical package in spectral domain with all necessary mathematical tools that, for the first time, extends the possibilities of spectral analysis to electromagnetic problems involving wedges immersed in an arbitrary linear medium, extendable to multiple penetrable angular regions. The theory is presented in an exhaustive way showing theoretical background, implementation and validation. The methodology is based on transverse equations for layered angular structures, the characteristic Green's function procedure, the Wiener-Hopf technique and the novel direct Fredholm factorization method that reduces GWHEs with multiple propagation constants to integral representations in a unique complex plane. Validation-through-examples is applied, starting from demonstrating effectiveness of direct Fredholm factorization applied to GWHEs in the scattering from a PEC wedge immersed in an isotropic medium and, ending with validation of functional equations of angular regions in arbitrary linear media with the analysis of a PEC half-plane immersed in particular anisotropic media. While numerically implementing the method, we observe that one of the main difficulties resides in the correct estimation of kernel functions for the presence of multivalued functions that need particular attention in their definition and calculation.

The proposed equations are interpreted using network formalism, providing a systematic perspective in particular for the analysis of complex scattering problems where the complexity of the geometry is broken into subdomains of canonical shape among which the angular regions immersed in/made of arbitrarily linear media.

The work presents significant advancements in the spectral analysis of electromagnetic problems from different mathematical, physical and engineering aspects: a first spectral method capable to handle scattering in arbitrary linear media with multiple propagation constants, a novel solution procedure of GWHEs in particular with multiple propagation constants (the Direct Fredholm Factorization), the network interpretation of spectral functional equations and related integral representations for angular regions filled by arbitrary linear media, the computation of the field at each point within the angular region avoiding spectral analytical extension and, the improvement of quality of approximate spectral solutions re-imposing GWHEs (named iteration).

The theoretical package is validated and ready for future applications.

Author Contributions:

V.D and G.L. co-developed the conceptualization, methodology, mathematics, formal analysis, investigation, validation, writing—original draft preparation, writing—review and editing, project administration, funding acquisition. All authors have read and agreed to the published version of the manuscript.

Funding: This research was funded by Italian Ministry of Universities and Research under PRIN Grant 2017NT5W7Z GREEN TAGS and Next Generation EU-PNRR M4C2-Inv 1.4–National Centre for HPC, Big Data and Quantum Computing (HPC)-Multiscale modeling and Engineering App.

Institutional Review Board Statement: Not applicable.

Informed Consent Statement: Not applicable.

Data Availability Statement: The original contributions presented in the study are included in the article comprehensive of the Appendix, further inquiries can be directed to the corresponding authors. The data presented in this study have been obtained by means of an in-house software code implementing the proposed method.

Conflicts of Interest: The authors declare no conflict of interest.

Appendix A Explicit form of expressions used in the main text

Appendix A contain details and supplemental to the main text, in particular explicit expressions that are cumbersome to be reported in the main text for readability and preserving completeness.

The explicit expressions of 4x4 matrices $\boldsymbol{M}_{yo}, \boldsymbol{M}_{y1}, \boldsymbol{M}_{y2}$ used in Section 2 at (4), i.e.

$$\boldsymbol{M}_{\boldsymbol{y}}(-j\alpha_o, \frac{\partial}{\partial x}) = \boldsymbol{M}_{yo} + (\frac{\partial}{\partial x})\boldsymbol{M}_{y1} + (\frac{\partial}{\partial x})^2\boldsymbol{M}_{y2} \tag{A1}$$

for an arbitrary linear media are in factorized form

$$\boldsymbol{M}_{yo} = \frac{j(\omega\boldsymbol{M}_{yo}^{(0)} + \alpha_o\boldsymbol{M}_{yo}^{(1)} + \alpha_o^2\boldsymbol{M}_{yo}^{(2)}/\omega)}{\epsilon_{yy}\mu_{yy} - \zeta_{yy}\xi_{yy}} \tag{A2}$$

$$\boldsymbol{M}_{yo}^{(0)} = \begin{pmatrix} \zeta_{xy}\zeta_{yz}\xi_{yy} - \zeta_{xz}\zeta_{yy}\xi_{yy} + \zeta_{xz}\mu_{yy}\epsilon_{yy} - \zeta_{yz}\mu_{xy}\epsilon_{yy} - \zeta_{xy}\mu_{yy}\epsilon_{yz} + \zeta_{yy}\mu_{xy}\epsilon_{yz} & -\zeta_{xx}\zeta_{yy}\xi_{yy} + \zeta_{xy}\zeta_{yx}\xi_{yy} - \zeta_{xy}\mu_{yy}\epsilon_{yx} + \zeta_{yy}\mu_{xy}\epsilon_{yx} + \zeta_{xx}\mu_{yy}\epsilon_{yy} - \zeta_{yx}\mu_{xy}\epsilon_{yy} \\ \zeta_{yy}\zeta_{zz}\xi_{yy} - \zeta_{yz}\zeta_{zy}\xi_{yy} + \zeta_{yz}\mu_{zy}\epsilon_{yy} - \zeta_{zz}\mu_{yy}\epsilon_{yy} - \zeta_{yy}\mu_{zy}\epsilon_{yz} + \zeta_{zy}\mu_{yy}\epsilon_{yz} & -\zeta_{yx}\zeta_{zy}\xi_{yy} + \zeta_{yy}\zeta_{zx}\xi_{yy} - \zeta_{yy}\mu_{zy}\epsilon_{yx} + \zeta_{zy}\mu_{yy}\epsilon_{yx} + \zeta_{yx}\mu_{zy}\epsilon_{yy} - \zeta_{zx}\mu_{yy}\epsilon_{yy} \\ -\zeta_{yz}\xi_{yy}\epsilon_{xy} + \mu_{yy}\epsilon_{xy}\epsilon_{yz} + \zeta_{yy}\xi_{yy}\epsilon_{xz} - \mu_{yy}\epsilon_{xz}\epsilon_{yy} + \zeta_{yz}\xi_{xy}\epsilon_{yy} - \zeta_{yy}\xi_{xy}\epsilon_{yz} & \zeta_{yy}\xi_{yy}\epsilon_{xx} - \mu_{yy}\epsilon_{xx}\epsilon_{yy} - \zeta_{yx}\xi_{yy}\epsilon_{xy} + \mu_{yy}\epsilon_{xy}\epsilon_{yx} - \zeta_{yy}\xi_{xy}\epsilon_{yx} + \zeta_{yx}\xi_{xy}\epsilon_{yy} \\ -\zeta_{yz}\xi_{zy}\epsilon_{yy} + \mu_{yy}\epsilon_{yy}\epsilon_{zz} + \zeta_{yy}\xi_{zy}\epsilon_{yz} - \mu_{yy}\epsilon_{yz}\epsilon_{zy} + \zeta_{yz}\xi_{yy}\epsilon_{zy} - \zeta_{yy}\xi_{yy}\epsilon_{zz} & \zeta_{yy}\xi_{zy}\epsilon_{yx} - \mu_{yy}\epsilon_{yx}\epsilon_{zy} - \zeta_{yx}\xi_{zy}\epsilon_{yy} + \mu_{yy}\epsilon_{yy}\epsilon_{zx} - \zeta_{yy}\xi_{yy}\epsilon_{zx} + \zeta_{yx}\xi_{yy}\epsilon_{zy} \end{pmatrix}$$

$$\begin{pmatrix} -\zeta_{xy}\mu_{yy}\xi_{yz} + \zeta_{xy}\mu_{yz}\xi_{yy} + \zeta_{yy}\mu_{xy}\xi_{yz} - \zeta_{yy}\mu_{xz}\xi_{yy} - \mu_{xy}\mu_{yz}\epsilon_{yy} + \mu_{xz}\mu_{yy}\epsilon_{yy} & \zeta_{xy}\mu_{yx}\xi_{yy} - \zeta_{xy}\mu_{yy}\xi_{yx} - \zeta_{yy}\mu_{xx}\xi_{yy} + \zeta_{yy}\mu_{xy}\xi_{yx} + \mu_{xx}\mu_{yy}\epsilon_{yy} - \mu_{xy}\mu_{yx}\epsilon_{yy} \\ -\zeta_{yy}\mu_{zy}\xi_{yz} + \zeta_{yy}\mu_{zz}\xi_{yy} + \zeta_{zy}\mu_{yy}\xi_{yz} - \zeta_{zy}\mu_{yz}\xi_{yy} - \mu_{yy}\mu_{zz}\epsilon_{yy} + \mu_{yz}\mu_{zy}\epsilon_{yy} & \zeta_{yy}\mu_{zx}\xi_{yy} - \zeta_{yy}\mu_{zy}\xi_{yx} - \zeta_{zy}\mu_{yx}\xi_{yy} + \zeta_{zy}\mu_{yy}\xi_{yx} + \mu_{yx}\mu_{zy}\epsilon_{yy} - \mu_{yy}\mu_{zx}\epsilon_{yy} \\ -\zeta_{yy}\xi_{xy}\xi_{yz} + \zeta_{yy}\xi_{xz}\xi_{yy} + \mu_{yy}\xi_{yz}\epsilon_{xy} - \mu_{yz}\xi_{yy}\epsilon_{xy} - \mu_{yy}\xi_{xz}\epsilon_{yy} + \mu_{yz}\xi_{xy}\epsilon_{yy} & \zeta_{yy}\xi_{xx}\xi_{yy} - \zeta_{yy}\xi_{xy}\xi_{yx} - \mu_{yx}\xi_{yy}\epsilon_{xy} + \mu_{yy}\xi_{yx}\epsilon_{xy} + \mu_{yx}\xi_{xy}\epsilon_{yy} - \mu_{yy}\xi_{xx}\epsilon_{yy} \\ -\zeta_{yy}\xi_{yy}\xi_{zz} + \zeta_{yy}\xi_{yz}\xi_{zy} + \mu_{yy}\xi_{zz}\epsilon_{yy} - \mu_{yz}\xi_{zy}\epsilon_{yy} - \mu_{yy}\xi_{yz}\epsilon_{zy} + \mu_{yz}\xi_{yy}\epsilon_{zy} & \zeta_{yy}\xi_{yx}\xi_{zy} - \zeta_{yy}\xi_{yy}\xi_{zx} - \mu_{yx}\xi_{zy}\epsilon_{yy} + \mu_{yy}\xi_{zx}\epsilon_{yy} + \mu_{yx}\xi_{yy}\epsilon_{zy} - \mu_{yy}\xi_{yx}\epsilon_{zy} \end{pmatrix} \tag{A3}$$

$$\boldsymbol{M}_{yo}^{(1)} = \begin{pmatrix} \zeta_{yz}\xi_{yy} - \mu_{yy}\epsilon_{yz} & \xi_{yy}(\zeta_{yx} - \zeta_{xy}) - \mu_{yy}\epsilon_{yx} + \mu_{xy}\epsilon_{yy} & \mu_{yz}\xi_{yy} - \mu_{yy}\xi_{yz} & -\mu_{yy}(\zeta_{xy} + \xi_{yx}) + \zeta_{yy}\mu_{xy} + \mu_{yx}\xi_{yy} \\ 0 & \zeta_{zy}\xi_{yy} - \mu_{zy}\epsilon_{yy} & 0 & \zeta_{zy}\mu_{yy} - \zeta_{yy}\mu_{zy} \\ \zeta_{yy}\epsilon_{yz} - \zeta_{yz}\epsilon_{yy} & \xi_{yy}\epsilon_{xy} + \zeta_{yy}\epsilon_{yx} - \epsilon_{yy}(\zeta_{yx} + \xi_{xy}) & \zeta_{yy}\xi_{yz} - \mu_{yz}\epsilon_{yy} & \zeta_{yy}(\xi_{yx} - \xi_{xy}) + \mu_{yy}\epsilon_{xy} + \mu_{yx}(-\epsilon_{yy}) \\ 0 & \zeta_{zy}\epsilon_{yy} - \xi_{yy}\epsilon_{zy} & 0 & \zeta_{yy}\xi_{zy} - \mu_{yy}\epsilon_{zy} \end{pmatrix} \tag{A4}$$

$$\boldsymbol{M}_{yo}^{(2)} = \begin{pmatrix} 0 & -\xi_{yy} & 0 & -\mu yy \\ 0 & 0 & 0 & 0 \\ 0 & \epsilon_{yy} & 0 & \zeta_{yy} \\ 0 & 0 & 0 & 0 \end{pmatrix} \tag{A5}$$

$$\boldsymbol{M}_{y1} = \frac{\boldsymbol{M}_{y1}^{(0)} + \alpha_o \boldsymbol{M}_{y1}^{(1)}/\omega}{\epsilon_{yy}\mu_{yy} - \zeta_{yy}\xi_{yy}} \tag{A6}$$

$$\boldsymbol{M}_{y1}^{(0)} = \begin{pmatrix} \mu_{xy}\epsilon_{yy} - \zeta_{xy}\xi_{yy} & 0 & \zeta_{yy}\mu_{xy} - \zeta_{xy}\mu_{yy} & 0 \\ -\zeta_{yz}\xi_{yy} + \zeta_{zy}\xi_{yy} - \mu_{zy}\epsilon_{yy} + \mu_{yy}\epsilon_{yz} & \mu_{yy}\epsilon_{yx} - \zeta_{yx}\xi_{yy} & -\zeta_{yy}\mu_{zy} + \zeta_{zy}\mu_{yy} + \mu_{yy}\xi_{yz} - \mu_{yz}\xi_{yy} & \mu_{yy}\xi_{yx} - \mu_{yx}\xi_{yy} \\ \xi_{yy}\epsilon_{xy} - \xi_{xy}\epsilon_{yy} & 0 & \mu_{yy}\epsilon_{xy} - \zeta_{yy}\xi_{xy} & 0 \\ \zeta_{yz}\epsilon_{yy} + \xi_{zy}\epsilon_{yy} + \zeta_{yy}(-\epsilon_{yz}) - \xi_{yy}\epsilon_{zy} & \zeta_{yx}\epsilon_{yy} - \zeta_{yy}\epsilon_{yx} & -\zeta_{yy}\xi_{yz} + \zeta_{yy}\xi_{zy} + \mu_{yz}\epsilon_{yy} + \mu_{yy}(-\epsilon_{zy}) & \mu_{yx}\epsilon_{yy} - \zeta_{yy}\xi_{yx} \end{pmatrix} \tag{A7}$$

$$\boldsymbol{M}_{y1}^{(1)} = \begin{pmatrix} -\xi_{yy} & 0 & -\mu_{yy} & 0 \\ 0 & \xi_{yy} & 0 & \mu_{yy} \\ \epsilon_{yy} & 0 & \zeta_{yy} & 0 \\ 0 & -\epsilon_{yy} & 0 & -\zeta_{yy} \end{pmatrix} \tag{A8}$$

$$\boldsymbol{M}_{y2} = \begin{pmatrix} 0 & 0 & 0 & 0 \\ -\xi_{yy} & 0 & -\mu_{yy} & 0 \\ 0 & 0 & 0 & 0 \\ \epsilon_{yy} & 0 & \zeta_{yy} & 0 \end{pmatrix} \tag{A9}$$

We note that the expressions of $\boldsymbol{M}_{yo}, \boldsymbol{M}_{y1}, \boldsymbol{M}_{y2}$ reported respectively in (A2),(A6),(A9) in factorized form with respect to α_o allows an immediate evaluation in case of normal incidence $\alpha_o = 0$, simplifying the expressions, by nullify the contribution of $\boldsymbol{M}_{yo}^{(1)}, \boldsymbol{M}_{yo}^{(2)}, \boldsymbol{M}_{y1}^{(1)}$.

References

1. Malyuzhinets, G. Excitation, reflection and emission of surface waves from a wedge with given face impedances. *Sov. Phys.-Dokl.* **1958**, *3*, 752–755.
2. Budaev, B.V.; Budaev, B.V. *Diffraction by wedges*; Number 322 in Pitman research notes in mathematics series, Longman Scientific & Technical: Harlow, 1995.
3. Senior, T.B.A.; Volakis, J.L. *Approximate boundary conditions in electromagnetics*; Number 41 in IEE electromagnetic waves series, Institution of Electrical Engineers: London, 1995.
4. Osipov, A.V.; Norris, A.N. The Malyuzhinets theory for scattering from wedge boundaries: a review. *Wave Motion* **1999**, *29*, 313–340. https://doi.org/10.1016/S0165-2125(98)00042-0.
5. Babich, V.M.; Lyalinov, M.A.; Grikurov, V.E. *Diffraction Theory: The Sommerfeld-Malyuzhinets Technique*; Alpha Science International, 2008.
6. Lyalinov, M.A.; Yan, Z.N. *Scattering of wedges and cones with impedance boundary conditions*; Mario Boella Series on Electromagnetism in Information and Communication Series, Raleigh, NC, USA: SciTech Publishing, 2013.
7. Oberhettinger, F. Diffraction of waves by a wedge. *Communications on Pure and Applied Mathematics* **1954**, *7*, 551–563. https://doi.org/10.1002/cpa.3160070306.
8. Osipov, A.V. On the method of Kontorovich–Lebedev's integrals for the problems of diffraction in sectorial media. In *Problems of Diffraction and Propagation of Waves*; 1993; Vol. 25, pp. 173–219.
9. Rawlins, A.D. Diffraction by, or Diffusion into, a Penetrable Wedge. *Proceedings: Mathematical, Physical and Engineering Sciences* **1999**, *455*, 2655–2686.
10. Salem, M.A.; Kamel, A.H.; Osipov, A.V. Electromagnetic fields in the presence of an infinite dielectric wedge. *Proceedings of the Royal Society A: Mathematical, Physical and Engineering Sciences* **2006**, *462*, 2503–2522. https://doi.org/10.1098/rspa.2006.1691.
11. Daniele, V.G. The Wiener–Hopf Technique for Impenetrable Wedges Having Arbitrary Aperture Angle. *SIAM Journal on Applied Mathematics* **2003**, *63*, 1442–1460. https://doi.org/10.1137/S0036139901400239.
12. Daniele, V.G.; Lombardi, G. Wiener-Hopf solution for impenetrable wedges at skew incidence. *IEEE Transactions on Antennas and Propagation* **2006**, *54*, 2472–2485. Publisher: IEEE.
13. Daniele, V.; Lombardi, G. The Wiener-Hopf Solution of the Isotropic Penetrable Wedge Problem: Diffraction and Total Field. *IEEE Transactions on Antennas and Propagation* **2011**, *59*, 3797–3818. https://doi.org/10.1109/TAP.2011.2163780.
14. Lombardi, G. Skew Incidence on Concave Wedge With Anisotropic Surface Impedance. *IEEE Antennas and Wireless Propagation Letters* **2012**, *11*, 1141–1145. Conference Name: IEEE Antennas and Wireless Propagation Letters, https://doi.org/10.1109/LAWP.2012.2219845.
15. Daniele, V.G.; Lombardi, G. *Scattering and Diffraction by Wedges 1: The Wiener-Hopf Solution - Theory*; John Wiley & Sons, 2020.
16. Daniele, V.G.; Lombardi, G. *Scattering and Diffraction by Wedges 2: The Wiener-Hopf Solution Advanced Applications*; John Wiley & Sons, 2020. https://doi.org/10.1002/9781119779452.
17. Daniele, V.G.; Lombardi, G.; Zich, R.S. Network representations of angular regions for electromagnetic scattering. *Plos One* **2017**, *12*, e0182763. https://doi.org/10.1371/journal.pone.0182763.
18. Sommerfeld, A. Mathematische Theorie der Diffraction. *Mathematische Annalen* **1896**, *47*, 317–374. https://doi.org/10.1007/BF01447273.
19. Daniele, V.; Lombardi, G. Fredholm factorization of Wiener-Hopf scalar and matrix kernels. *Radio Science* **2007**, *42*, 1–19. https://doi.org/10.1029/2007RS003673.
20. Daniele, V.G. Rotating Waves in the Laplace Domain for Angular Regions. *Electromagnetics* **2003**, *23*, 223–236. https://doi.org/10.1080/02726340390197485.
21. Seshadri, S.; Rajagopal, A. Diffraction by a perfectly conducting semi-infinite screen in an anisotropic plasma. *IEEE Transactions on Antennas and Propagation* **1963**, *11*, 497–502. https://doi.org/10.1109/TAP.1963.1138071.
22. Jull, E.V. Diffraction by a conducting half-plane in an anisotropic plasma. *Canadian Journal of Physics* **1964**, *42*, 1455–1468. Publisher: NRC Research Press, https://doi.org/10.1139/p64-133.
23. Felsen, L.B. Propagation and diffraction in uniaxially anisotropic regions. Part 1. Theory. *Proceedings of the Institution of Electrical Engineers* **1964**, *111*, 445–453. https://doi.org/10.1049/piee.1964.0081.
24. Felsen, L.B. Propagation and diffraction in uniaxially anisotropic regions. Part 2. Applications. *Proceedings of the Institution of Electrical Engineers* **1964**, *111*, 454–464. https://doi.org/10.1049/piee.1964.0082.
25. Williams, W.E. Electromagnetic Diffraction in an Anisotropic Medium. *IMA Journal of Applied Mathematics* **1966**, *2*, 186–196. https://doi.org/10.1093/imamat/2.2.186.
26. Hurd, R.A.; Przeździecki, S. Diffraction by a half-plane perpendicular to the distinguished axis of a gyrotropic medium. *Journal of Mathematical Physics* **1976**, *17*, 1838–1847. https://doi.org/10.1063/1.522804.
27. Przedziecki, S.; Hurd, R.A. Diffraction by a half-plane perpendicular to the distinguished axis of a general gyrotropic medium. *Canadian Journal of Physics* **1977**, *55*, 305–324. https://doi.org/10.1139/p77-045.
28. Hurd, R.; Przedziecki, S. Half-plane diffraction in a gyrotropic medium. *IEEE Transactions on Antennas and Propagation* **1985**, *33*, 813–822. https://doi.org/10.1109/TAP.1985.1143679.
29. Przedziecki, S. Half-plane diffraction in a chiral medium. *Wave Motion* **2000**, *32*, 157–200. https://doi.org/10.1016/S0165-2125(00)00037-8.

30. Daniele, V.; Graglia, R.D. Diffraction by an imperfect half plane in a bianisotropic medium. *Radio Science* **2007**, *42*, 1–16. https://doi.org/10.1029/2007RS003674.
31. Tellegen, B.D. The gyrator, a new electric network element. *Philips Res. Rep* **1948**, *3*, 81–101.
32. Cheng, D.; Kong, J.A. Covariant descriptions of bianisotropic media. *Proceedings of the IEEE* **1968**, *56*, 248–251. https://doi.org/10.1109/PROC.1968.6268.
33. Lindell, I.; Sihvola, A.; Tretyakov, S.; Viitanen, A.J. *Electromagnetic Waves in Chiral and Bi-isotropic Media*; Antennas and Propagation Library, Artech House, 1994.
34. Olyslager, F. The behavior of electromagnetic fields at edges in bi-isotropic and bi-anisotropic materials. *IEEE Transactions on Antennas and Propagation* **1994**, *42*, 1392–1397. https://doi.org/10.1109/8.320745.
35. Vashtalov, S.; Fisanov, V. Diffraction of a plane wave from a wedge in a chiral medium. *Russian Physics Journal* **1993**, *36*, 982–989.
36. Daniele, V.G.; Lombardi, G.; Zich, R.S. The Electromagnetic Field for a PEC Wedge Over a Grounded Dielectric Slab: 2. Diffraction, Modal Field, Surface Waves, and Leaky Waves. *Radio Science* **2017**, *52*, 1492–1509. https://doi.org/10.1002/2017RS006388.
37. Daniele, V.; Lombardi, G.; Zich, R.S. The Double PEC Wedge Problem: Diffraction and Total Far Field. *IEEE Transactions on Antennas and Propagation* **2018**, *66*, 6482–6499. https://doi.org/10.1109/TAP.2018.2877260.
38. Daniele, V.; Lombardi, G.; Zich, R.S. Radiation and Scattering of an Arbitrarily Flanged Dielectric-Loaded Waveguide. *IEEE Transactions on Antennas and Propagation* **2019**, *67*, 7569–7584. https://doi.org/10.1109/TAP.2019.2948494.
39. Daniele, V.; Zich, R.S. The Scattering by an Half-Plane Embedded in Stratified Media. Network Methods: Electromagnetics vs Elasticity. *Memorie dell'Accademia delle Scienze di Torino* **2022**, *1*, 5–52.
40. Daniele, V.G.; Zich, R.S. *The Wiener-Hopf Method in Electromagnetics*; Mario Boella Series on Electromagnetism in Information and Communication Series, Raleigh, NC, USA: SciTech Publishing, 2014.
41. Daniele, V.G.; Lombardi, G. The generalized Wiener–Hopf equations for wave motion in angular regions: electromagnetic application. *Proceedings of the Royal Society A: Mathematical, Physical and Engineering Sciences* **2021**, *477*, 20210040, 1–27. https://doi.org/10.1098/rspa.2021.0040.
42. Bresler A.D., M.N. OperatorMethods in Electromagnetic Field Theory, Report R-495,56, PIB425,MRI, 1956.
43. Felsen, L.B.; Marcuvitz, N. *Radiation and Scattering of Waves*; Prentice-Hall: Englewood Cliffs, NJ, 1973.
44. Daniele, V.G.; Zich, R.S. Radiation by arbitrary sources in anisotropic stratified media. *Radio Science* **1973**, *8*, 63–70. https://doi.org/10.1029/RS008i001p00063.
45. Noble, B. *Methods Based on the Wiener-Hopf Technique for the Solution of Partial Differential Equations*; Pergamon Press, 1958.
46. DeRusso, P.; Roy, R.; Charles, M. *State Variables for Engineers*; Wiley, 1965.
47. Kantorovich, L.V. *Approximate methods of higher analysis*; Groningen, The Netherlands: Noordhoff, 1958.
48. Lombardi, G. Design of quadrature rules for Müntz and Müntz-logarithmic polynomials using monomial transformation. *International Journal for Numerical Methods in Engineering* **2009**, *80*, 1687–1717. https://doi.org/10.1002/nme.2684.
49. Lombardi, G.; Papapicco, D. Quadrature of functions with endpoint singular and generalised polynomial behaviour in computational physics. *Computer Physics Communications* **2024**, *299*, 109124,1–17. https://doi.org/10.1016/j.cpc.2024.109124.